Supporting Information

Table of Contents

1. Instruments and Materials

^{1}H NMR (500 MHz) spectra were measured by a Bruker AVANCE-500 spectrometer, and chemical shifts were reported on the delta scale in ppm relative to $CHCl_3$ as an internal reference (δ = 7.26 ppm). UV/Vis absorption spectra were recorded on a Shimadzu UV-3600 spectrometer. MALDI-TOF mass spectra were obtained with a Bruker ultrafleXtreme MALDI-TOF/TOF spectrometer with matrix. X-ray data were taken on an Agilent SuperNova, X-ray diffractometer equipped with a large area CCD detector. Redox potentials were measured by cyclic voltammetry on a CHI900 scanning electrochemical microscope. Unless otherwise noted, materials obtained from commercial suppliers were used without further purification. Redox potentials were measured by the cyclic voltammetry and differential pulse voltammetry method on an ALS660 electrochemical analyzed model (Solvent: CH_2Cl_2, Electrolyte: 0.1 M $^n Bu_4NPF_6$, Working electrode: glassy carbon, Reference electrode: $Ag/AgNO_3$, Counter electrode: Pt wire, Scan rate: 0.05 V/s, External reference: ferrocene/ferrocenium cation). CH_2Cl_2 passed through an alumina column was used for electrochemical analysis.

2. Experimental Procedure

Synthesis of 6 and 7.

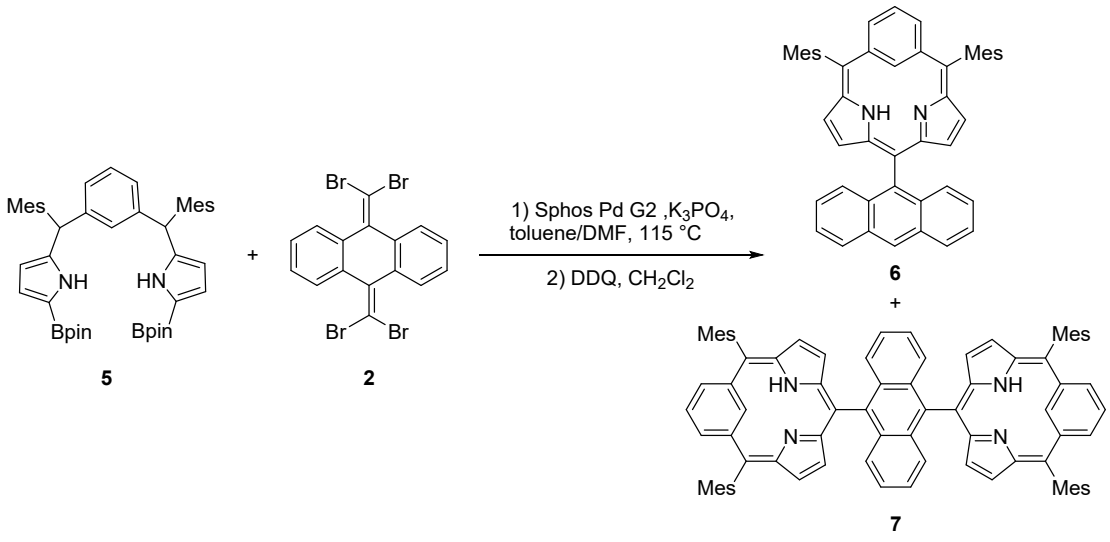

A toluene–DMF solution (5 mL/2.5 mL) of *α*,*α*'-diborylbenzitripyrrane **5** (434.6 mg, 0.6 mmol), 9,10-bis(dibromomethylene)-9,10-dihydroanthracene **2** (208.0 mg, 0.4 mmol), SPhos Pd G2 (28.8 mg, 0.04 mmol), and K_3PO_4 (426.6 mg, 2.0 mmol) was degassed through three freeze-pump-thaw cycles, and the reaction flask was purged with argon. The resulting mixture was refluxed for 48 h. The reaction mixture was diluted with $CHCl_3$, washed with water, and dried over anhydrous sodium sulfate. After the solvent was removed, an excess amount of DDQ was added to the mixture in CH_2Cl_2 and the resulting solution was stirred for another 10 min. The reaction mixture was passed through a short alumina column with CH_2Cl_2 as an eluent. Evaporation of the solvent followed by column chromatography through silica gel (CH_2Cl_2/*n*-hexane as an eluent) and recrystallization from *n*-hexane gave **6** as green solids (14.7 mg, 0.011 mmol, 5.6% yield) and **7** (12.3 mg, 0.011 mmol, 2.7%) as green solids.

6: ^{1}H NMR (500 MHz, $CDCl_3$) δ = 19.54 (s, 1H, N-H), 8.52 (s, 1H, anthryl-H), 8.41 (d, J = 8.5 Hz, 1H, anthryl-H), 8.05 (m, 2H, anthryl-H), 7.81 (d, J = 8.5 Hz, 1H, anthryl-H), 7.47 (m, 2H, anthryl-H), 7.40 (t, 1H, Ph-H), 7.36 (m, 2H, anthryl-H), 7.07 (d, J = 7 Hz, 2H, phenyl-H), 7.06 (s, 2H, Mes-*m*-H), 6.93 (s, 2H, Mes-*m*-H), 6.67 (d, J = 4.5 Hz, 2H, pyrrole-H), 6.65 (s, 1H, phenyl-H), 6.18 (d, J = 4.5 Hz, 2H, pyrrole-H), 2.46 (s, 6H, Me-H), 2.37 (s, 6H, Me-H), and 2.02 (s, 6H, Me-H) ppm. λ_{max} (ε [$M^{-1}cm^{-1}$]) = 385 (20100), 670 (4700) nm. (HR-MS (MALDI-TOF-MS): *m/z* = 656.3152, calcd for $(C_{49}H_{40}N_2)^+$ = 656.3186([*M*]$^+$).

7: ^{1}H NMR (500 MHz, $CDCl_3$) δ = 19.63-19.59 (s+s, 2H, N-H), 8.53-8.49 (m, 2H, anthryl-H), 7.91-7.89 (m, 2H, anthryl-H), 7.43-7.36 (m, 6H, anthryl-H+phenyl-H), 7.11-7.09 (m, 8H, anthryl-H+phenyl-H), 6.96 (s, 4H, Ar-*m*-H), 6.72 (d, J = 4.5 Hz, 4H, pyrrole-H), 6.70+6.69 (s+s, 2H, inner Phenyl-H), 6.32-6.28 (m, 4H, pyrrole-H), 2.49 (s, 12H, Me-H), 2.40 (s, 12H, Me-H), and 2.06 (s, 12H, Me-H) ppm. λ_{max} (ε [$M^{-1}cm^{-1}$]) = 392 (45400), 670 (11700) nm. HR-MS (MALDI-TOF-MS): *m/z* = 1134.5505, calcd for $(C_{84}H_{70}N_4)^+$ = 1134.5595([M]$^+$).

Synthesis of 8.

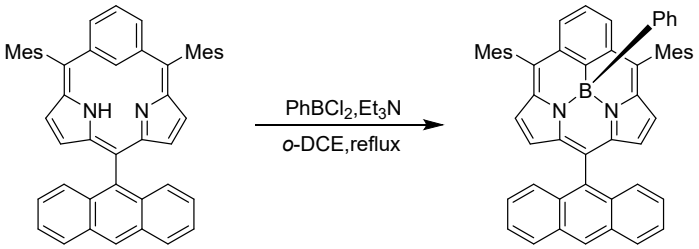

6 8

Compound **6** (20 mg, 0.030 mmol) was dissolved in dry 1,2-dichlorobenzene (5 mL) in a round-bottomed 50 mL flask containing a magnetic bar, and the resulting solution was refluxed in an inert atmosphere for about 10 min. Dry triethyl amine (0.1 mL) were added to the solution and the heating was continued for 10 min. Freshly distilled $PhBCl_2$ (0.1 mL) was added. The progress of the reaction was monitored by TLC. After the completion of the reaction, the reaction mixture was diluted with CH_2Cl_2, washed with water, and dried over anhydrous sodium sulfate. After the solvent was removed, the product was purified by silica-gel column chromatography (CH_2Cl_2/*n*-hexane as an eluent) to give **8** (10.3 mg, 0.014 mmol, 46% yield) as yellow solids.

8: ^{1}H NMR (500 MHz, $CDCl_3$) δ = 8.53 (s, 1H, anthryl-H), 8.07 (d, J = 8.0 Hz, 1H, anthryl-H), 8.02 (d, J = 8.0 Hz, 1H, anthryl-H), 7.92-7.88 (m, 2H, anthryl-H), 7.45-7.42 (m, 2H, anthryl-H), 7.36 (t, 1H, phenyl-H), 7.21-7.09(m, 9H, anthryl-H+axial phenyl-H+phenyl-H), 6.99(s, 2H, Mes-*m*-H), 6.97(s, 2H, Mes-*m*-H), 6.64(d, J = 4.5 Hz, 2H, pyrrole-H), 6.11(d, J = 4.5 Hz, 2H, pyrrole-H), 2.38 (s, 6H, Me-H), 2.21 (s, 6H, Me-H), and 2.03 (s, 6H, Me-H). λ_{max} (ε [$M^{-1}cm^{-1}$]) = 388 (24200) and 803 (1600) nm. (HR-MS (MALDI-TOF-MS): *m/z* = 665.2687, calcd for $(C_{49}H_{38}BN_2)^+$ = 665.3131([*M*-Ph]$^+$).

Synthesis of 9.

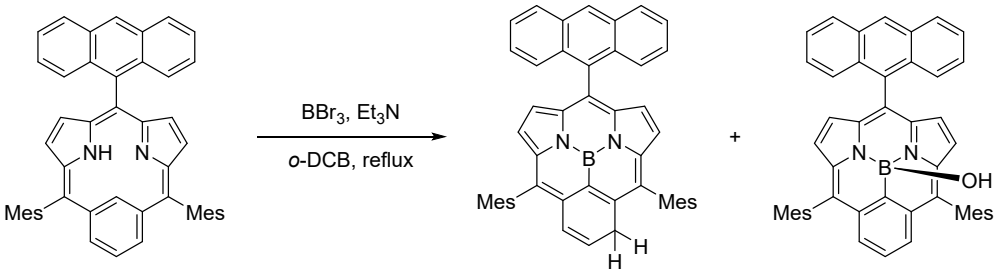

6 **9** **10**

Compound **6** (20 mg, 0.030 mmol) was dissolved in dry 1,2-dichlorobenzene (5 mL) in a round-bottomed 50 mL flask containing a magnetic bar, and the resulting solution was refluxed in an inert atmosphere for about 10 min. Dry triethyl amine (0.1 mL) were added to the solution and the heating was continued for 10 min. BBr_3 (0.1 mL) was added. The progress of the reaction was monitored by TLC. After the completion of the reaction, the reaction mixture was diluted with CH_2Cl_2, washed with water, and dried over anhydrous sodium sulfate. After the solvent was removed, the product was purified by silica-gel column chromatography using CH_2Cl_2/*n*-hexane as an eluent to give **9** (10.2 mg，0.015 mmol, 51% yield) as red solids and **10** (4.5 mg, 0.007 mmol, 21% yield) as green solids.

9：^{1}H NMR (500 MHz, $CDCl_3$) δ = 8.75 (s, 1H, anthryl-H), 8.18 (d, *J* = 8.5 Hz, 2H, anthryl-H), 7.58-7.54 (m, 4H, pyrrole-H+anthryl-H), 7.45-7.42 (m, 3H, pyrrole-H+anthryl-H), 7.40 (d, *J* = 4.5 Hz, 1H, pyrrole-H), 7.17 (t, 2H, anthryl-H), 7.15 (s, 2H, Mes-*m*-H), 7.11 (s, 2H, Mes-*m*-H), 6.67(d, *J* = 10.1 Hz, 1H, allyl-H), 6.25-6.21 (dt, 1H, allyl-H), 4.11 (br, 2H, allyl-H), 2.46 (s, 6H, Me-H), 2.03 (s, 6H, Me-H), and 1.98 (s, 6H, Me-H). λ_{max} (ε [$M^{-1}cm^{-1}$]) = 335 (58700), 356 (54700), 546 (29500) nm. (HR-MS (MALDI-TOF-MS): *m/z* = 656.2832, calcd for $(C_{49}H_{38}BN_2)^+$ = 656.3131([*M*-H]$^+$).

10: ^{1}H NMR (500 MHz, $CDCl_3$) δ = 8.59 (s, 1H, anthryl-H), 8.35 (d, *J* = 8.5 Hz, 1H, anthryl-H), 8.09-8.07 (m, 2H, anthryl-H), 7.64 (d, *J* = 8.5 Hz, 1H, anthryl-H), 7.52-7.50 (m, 2H, anthryl-H), 7.44 (t, 1H, phenyl-H), 7.31-7.21 (m, 4H, anthryl-H+phenyl-H), 7.04 (s, 2H, Mes-*m*-H), 6.97 (s, 2H, Mes-*m*-H), 6.71 (d, *J* = 5.0 Hz, 2H, pyrrole-H), 6.20 (d, *J* = 5.0 Hz, 2H, pyrrole-H), 2.43 (s, 6H, Me-H), 2.39

(s, 6H, Me-H), and 1.99 (s, 6H, Me-H) ppm. (The O*H* was not observed.) (HR-MS (MALDI-TOF-MS): *m/z* = 664.3184, calcd for $(C_{49}H_{38}BN_2)^+$ = 664.3159 ([*M*-OH]$^+$).

Synthesis of 10.

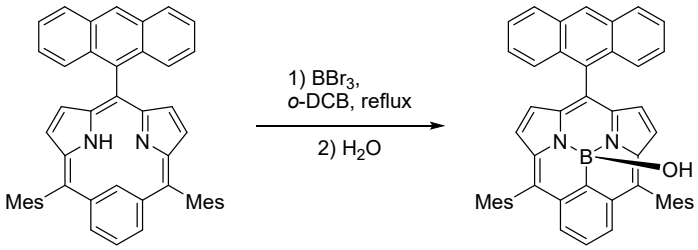

6 **10**

Compound **6** (20 mg, 0.030 mmol) was dissolved in dry 1,2-dichlorobenzene (5 mL) in a round-bottomed 50 mL flask containing a magnetic bar, and the resulting solution was refluxed in an inert atmosphere for about 10 min. BBr_3 (0.1 mL) was added. The progress of the reaction was monitored by TLC. After the completion of the reaction, the reaction mixture was diluted with CH_2Cl_2, washed with water, and dried over anhydrous sodium sulfate. After the solvent was removed, the product was purified by column chromatography on silica-gel (CH_2Cl_2/*n*-hexane as an eluent) to give **10** (19.5 mg, 0.029 mmol, 95% yield).

Synthesis of 11.

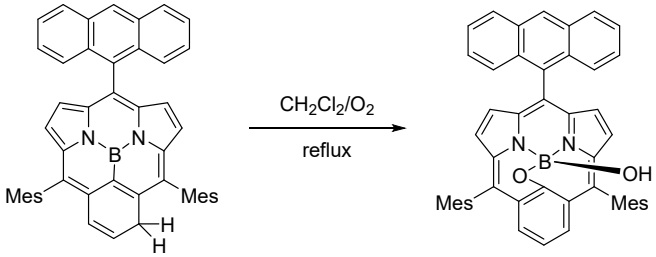

9 **11**

Compound **9** (20 mg, 0.030 mmol) was dissolved in dry CH_2Cl_2 (10 mL) in a round-bottomed 50 mL flask containing a magnetic bar, and the resulting solution was refluxed in the air for about 48 h. The progress of the reaction was

monitored by TLC. After the completion of the reaction, the reaction mixture was diluted with CH_2Cl_2, washed with water, and dried over anhydrous sodium sulfate. After the solvent was removed, the product was purified by column chromatography on silica-gel (CH_2Cl_2/*n*-hexane as an eluent) to give **11** (20.3 mg, 0.029 mmol, 97% yield).

11: ^{1}H NMR (500 MHz, $CDCl_3$) δ = 8.64 (d, J = 8.5 Hz, 1H, anthryl-H), 8.56 (s, 1H, anthryl-H), 8.10-8.05 (m, 2H, anthryl-H), 7.52-7.50 (m, 2H, anthryl-H), 7.43-7.39 (m, 2H, anthryl-H), 7.26 (m, 1H, anthryl-H), 7.04 (s, 2H, Mes-*m*-H), 6.99 (s, 2H, Mes-*m*-H), 6.89 (t, 1H, phenyl-H), 6.66-6.64 (m, 4H, phenyl-H+pyrrole+H), 6.17 (d, J = 4.5 Hz, 2H, pyrrole-H), 2.47 (s, 6H, Me-H), 2.38 (s, 6H, Me-H), and 2.00 (s, 6H, Me-H). (The O*H* was not observed.) λ_{max} (ε [$M^{-1}cm^{-1}$]) = 388 (28100) and 654 (3400) nm. (HR-MS (MALDI-TOF-MS): *m/z* = 698.3118, calcd for $(C_{49}H_{39}BN_2O_2)^+$ = 698.3107 ([*M*]$^+$).

Synthesis of 12.

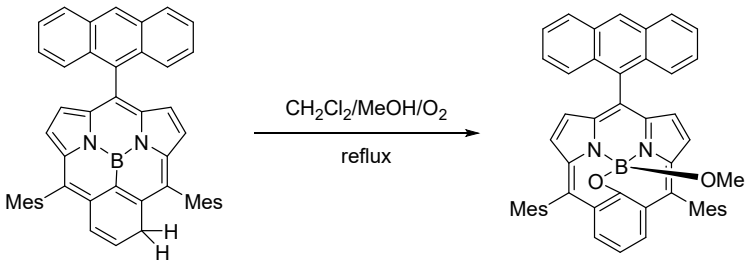

9 **12**

Compound **9** (20 mg, 0.030 mmol) was dissolved in dry CH_2Cl_2/MeOH (10/2 mL) in a round-bottomed 50 mL flask containing a magnetic bar, and the resulting solution was refluxed in the air for 48 h. The progress of the reaction was monitored by TLC. After the completion of the reaction, the reaction mixture was diluted with CH_2Cl_2, washed with water, and dried over anhydrous sodium sulfate. After the solvent was removed, the product was purified by column chromatography on silica-gel (CH_2Cl_2/*n*-hexane as an eluent) to give **12** (18.4 mg, 0.026 mmol, 86% yield).

12: ^{1}H NMR (500 MHz, $CDCl_3$) δ = 8.59 (d, J = 8.5 Hz, 1H, anthryl-H), 8.56 (s,

1H, anthryl-H), 8.07-8.05 (m, 2H, anthryl-H), 7.52-7.50 (m, 2H, anthryl-H), 7.45-7.40 (m, 2H, anthryl-H), 7.26 (m, 1H, anthryl-H), 7.04 (s, 2H, Mes-*m*-H), 6.99 (s, 2H, Mes-*m*-H), 6.89 (t, 1H, phenyl-H), 6.65-6.63 (m, 4H, phenyl-H+pyrrole+H), 6.20 (d, J = 4.5 Hz, 2H, pyrrole-H), 3.22 (s, 3H, MeO-H), 2.50 (s, 6H, Me-H), 2.38 (s, 6H, Me-H), and 2.01 (s, 6H, Me-H). λ_{max} (ε [$M^{-1}cm^{-1}$]) = 388 (31800) and 652 (3900) nm. (HR-MS (MALDI-TOF-MS): *m/z* = 712.3277, calcd for $(C_{50}H_{41}BN_2O_2)^+$ = 712.3264 ([*M*]$^+$).

3. Spectra of Compounds

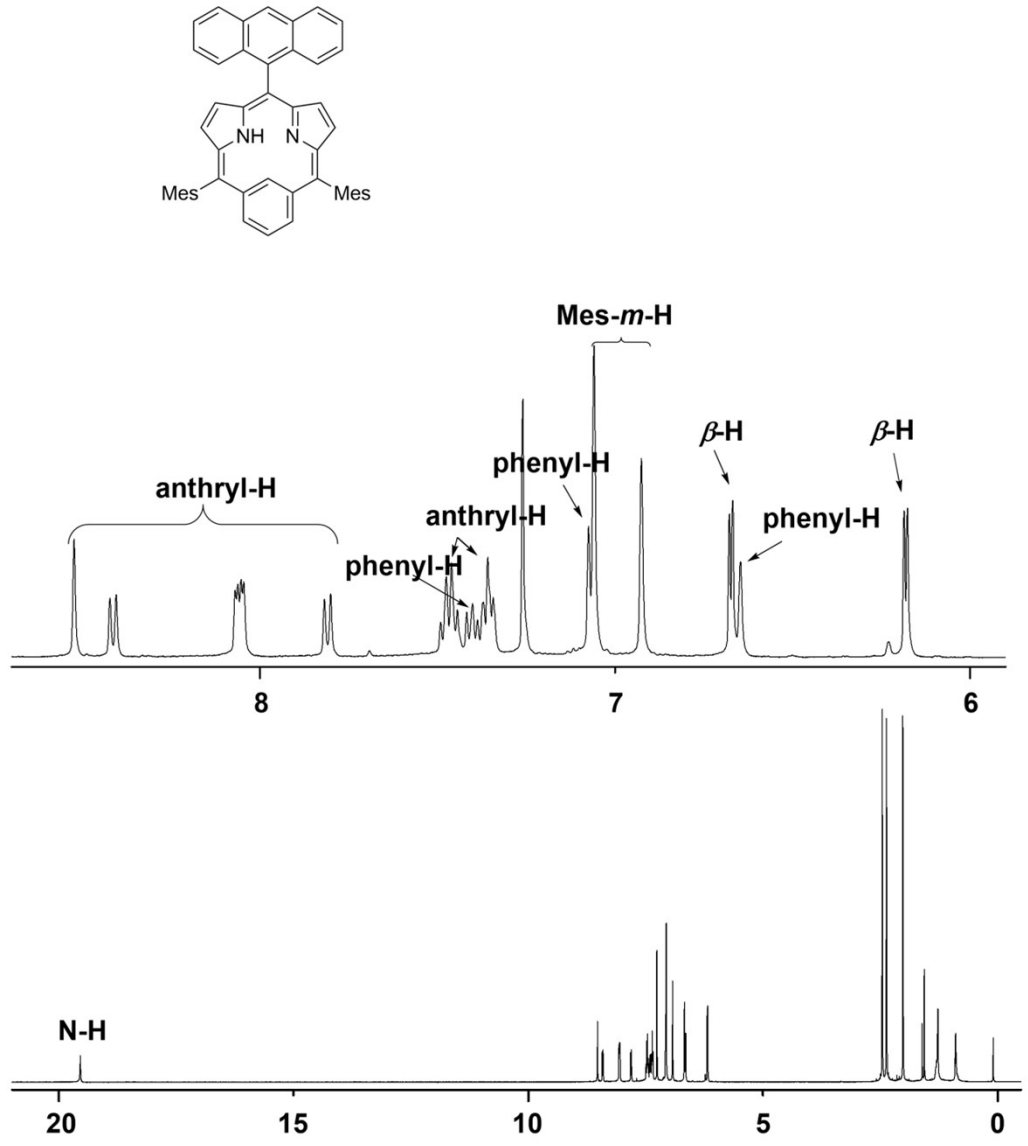

Figure S1. ^{1}H NMR spectrum of **6** in $CDCl_3$.

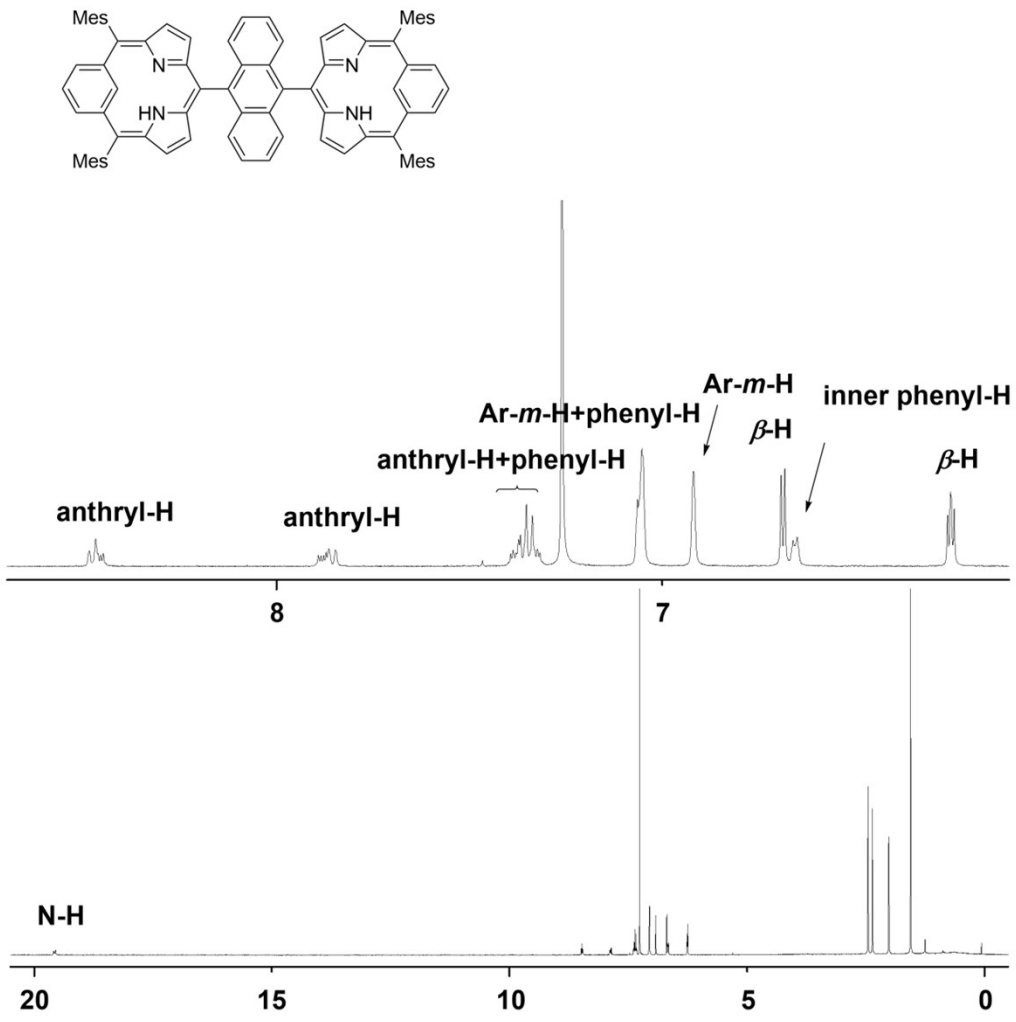

Figure S2. ^{1}H NMR spectrum of **7** in $CDCl_3$.

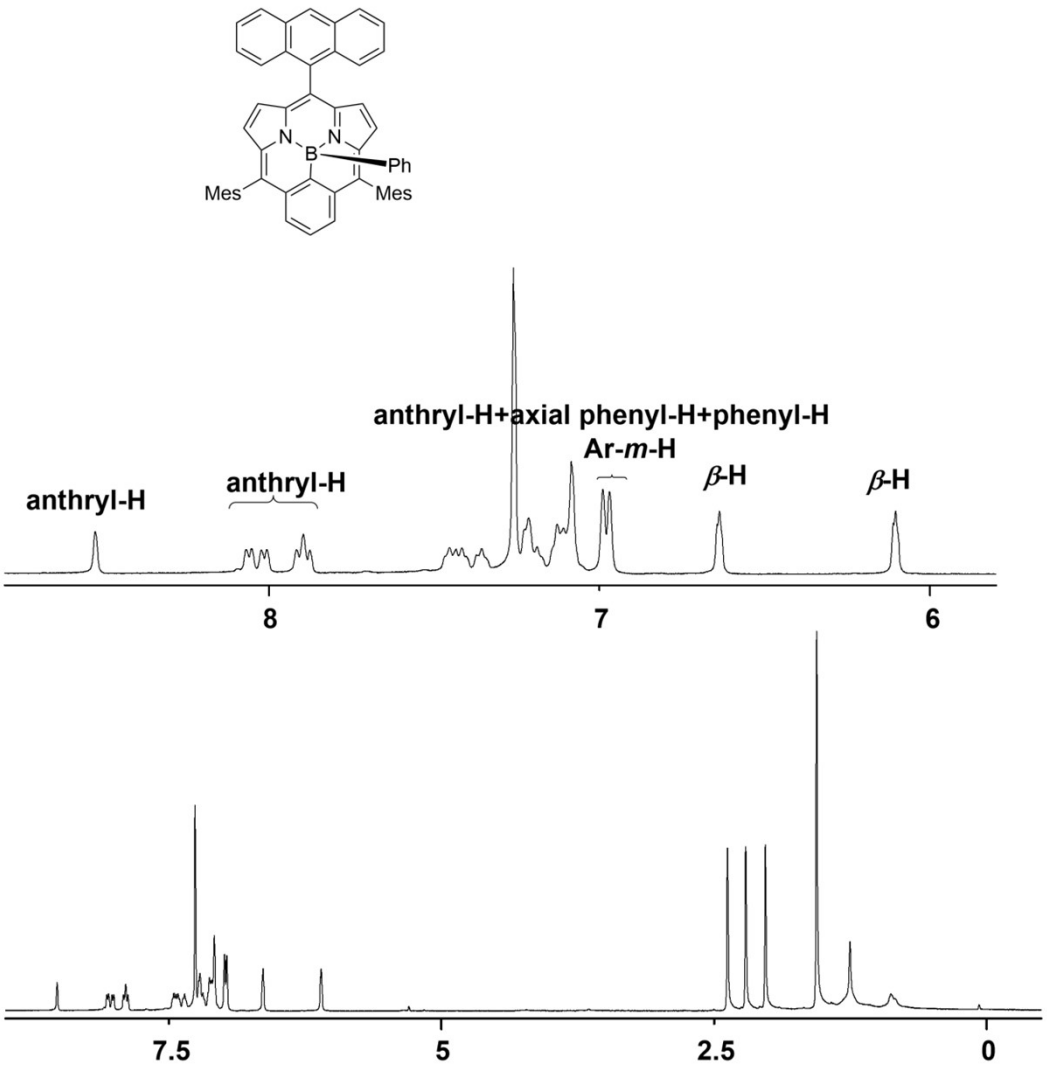

Figure S3. ^{1}H NMR spectrum of **8** in $CDCl_3$.

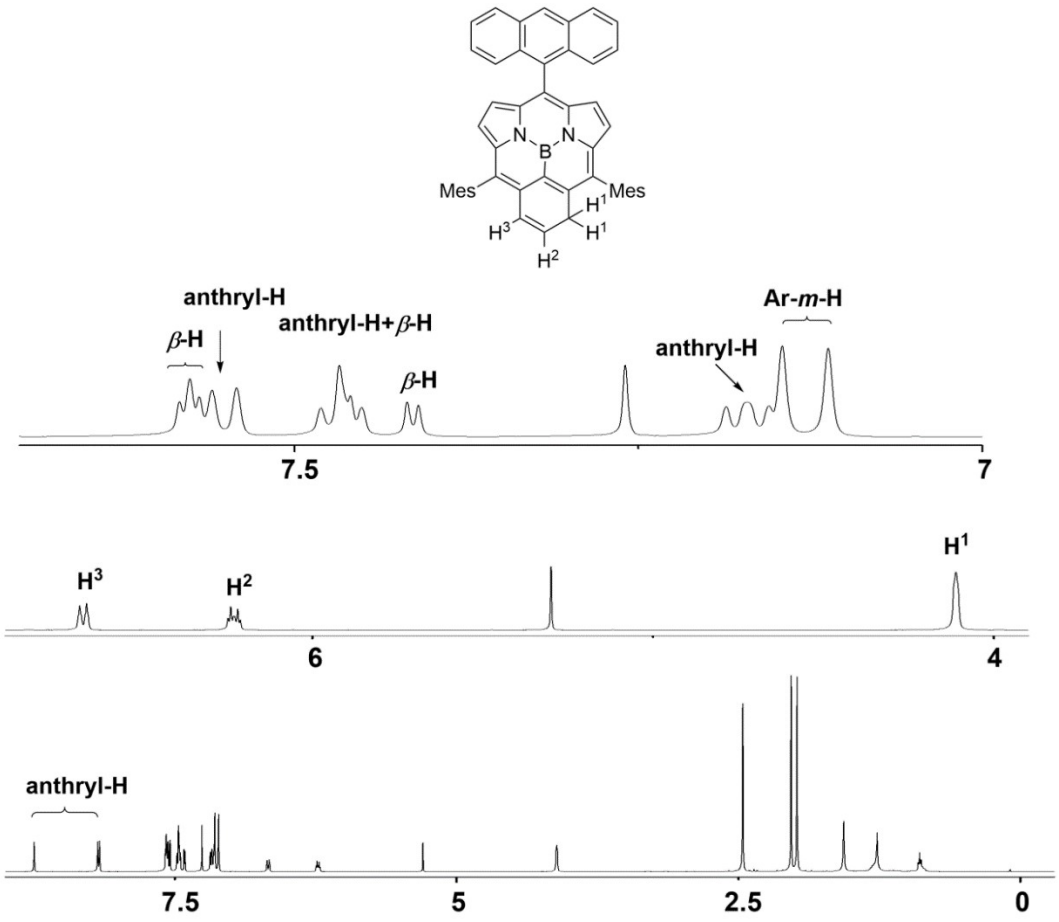

Figure S4. ^{1}H NMR spectrum of **9** in $CDCl_3$.

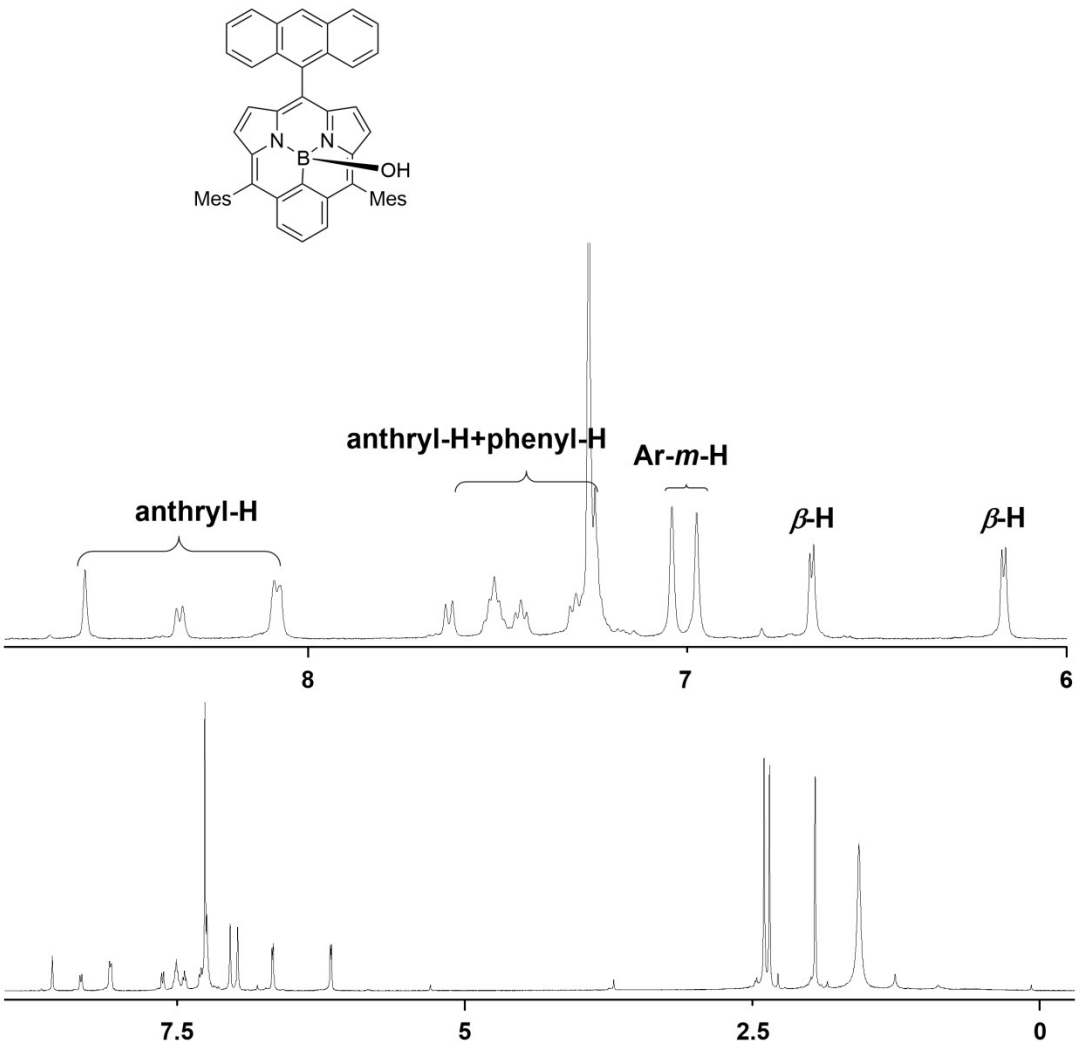

Figure S5. ^{1}H NMR spectrum of **10** in $CDCl_3$.

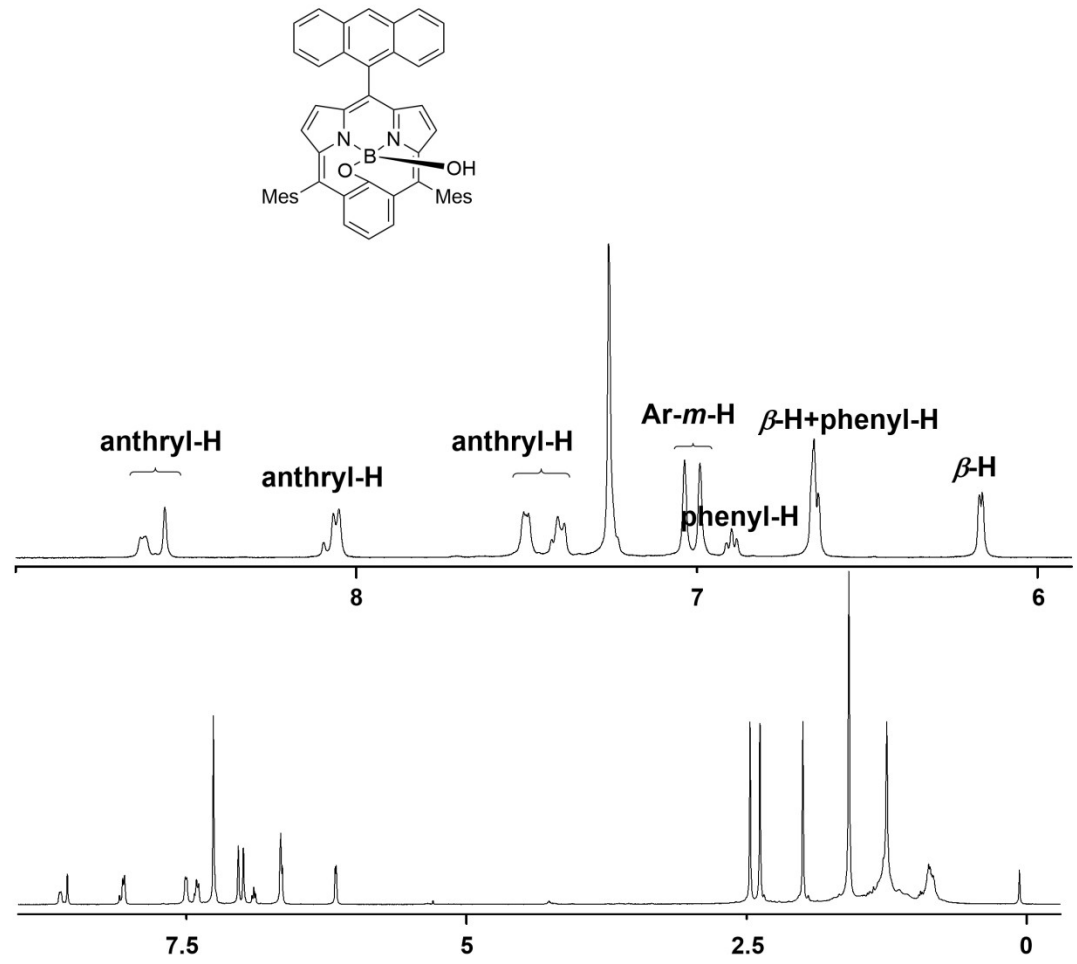

Figure S6. ^{1}H NMR spectrum of **11** in $CDCl_3$.

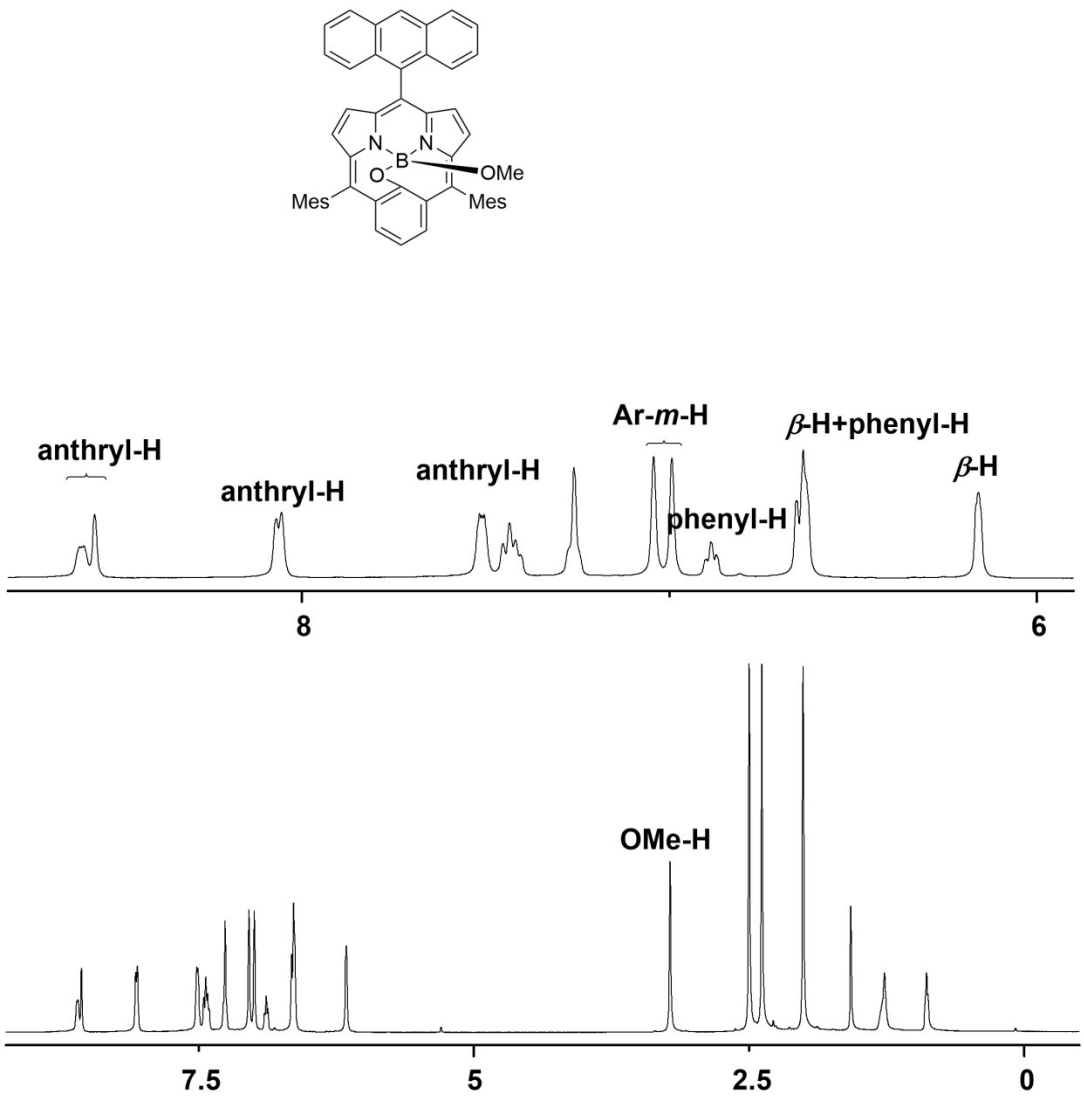

Figure S7. ^{1}H NMR spectrum of **12** in $CDCl_3$.

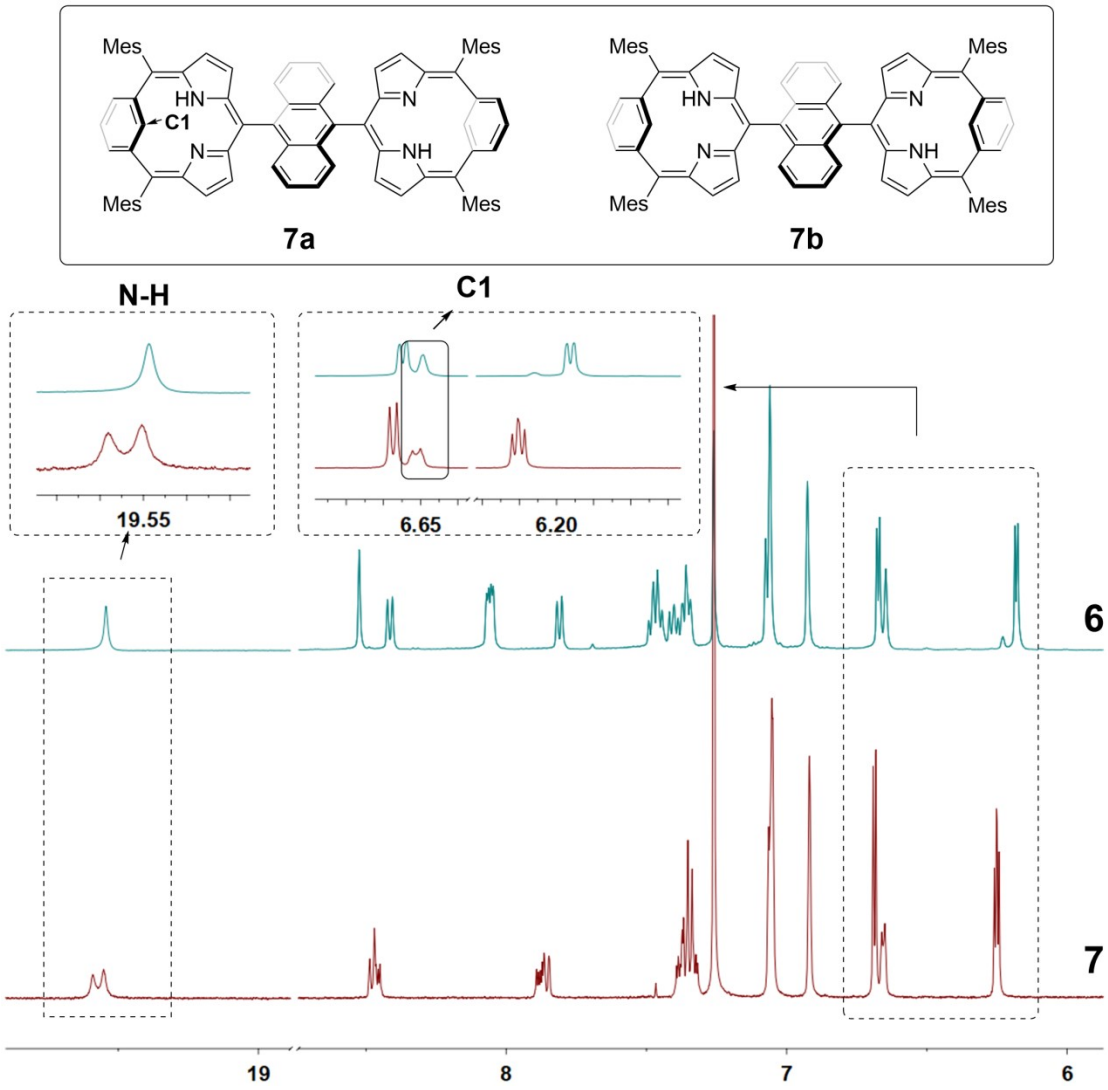

Figure S8. Comparison of ^{1}H NMR spectra of **6** and **7** in $CDCl_3$.

Mass Spectra

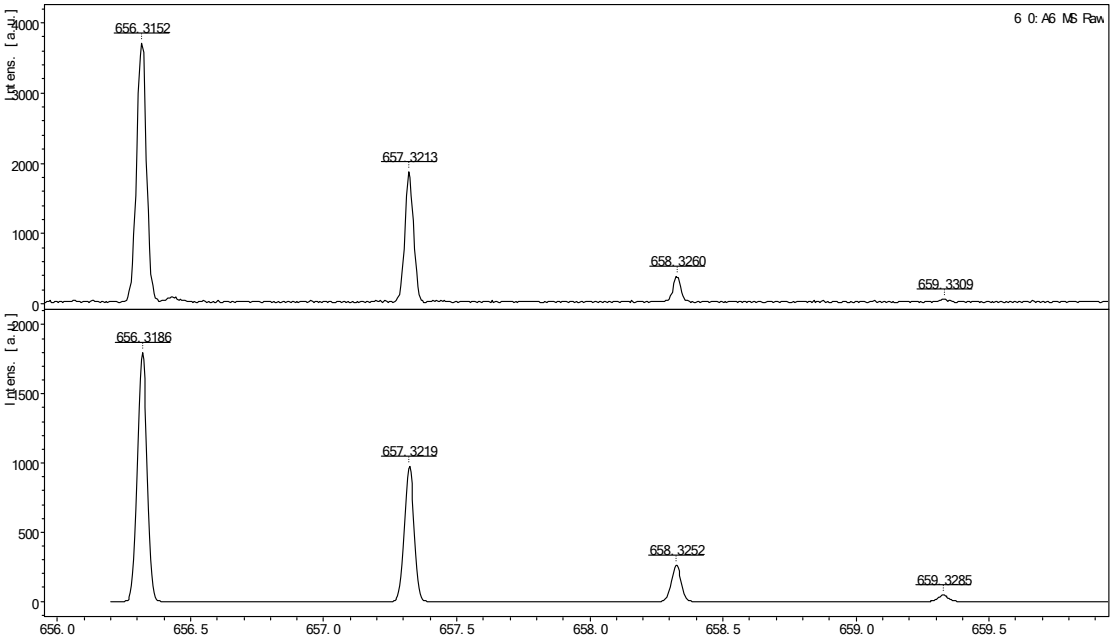

Figure S9. MALDI-TOF-MS of **6**. (Top: observed; Bottom: simulated)

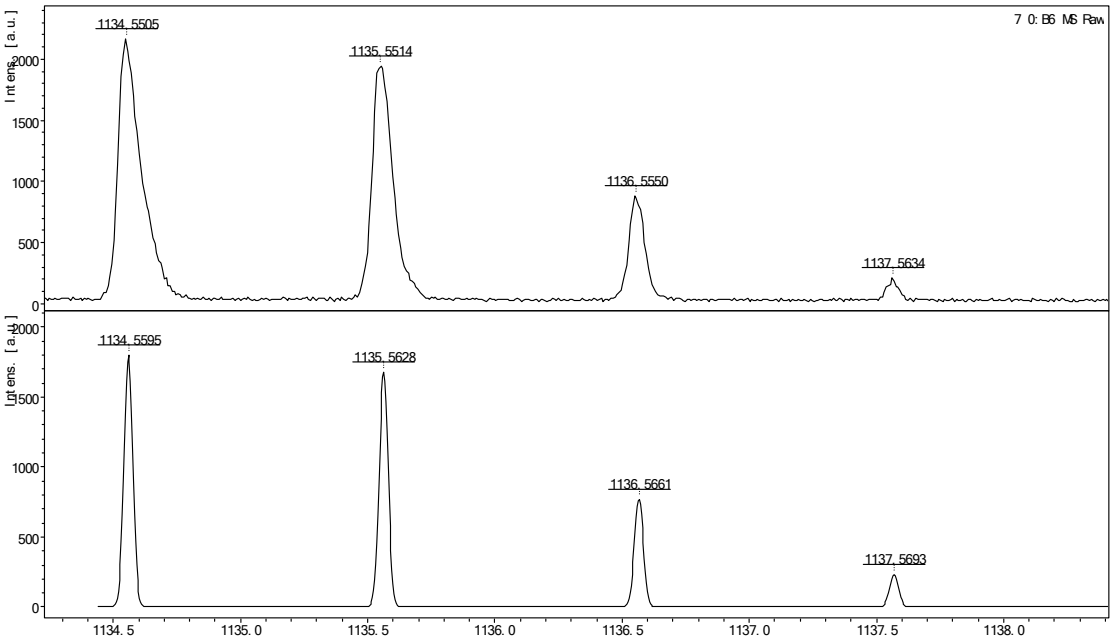

Figure S10. MALDI-TOF-MS of **7**. (Top: observed; Bottom: simulated)

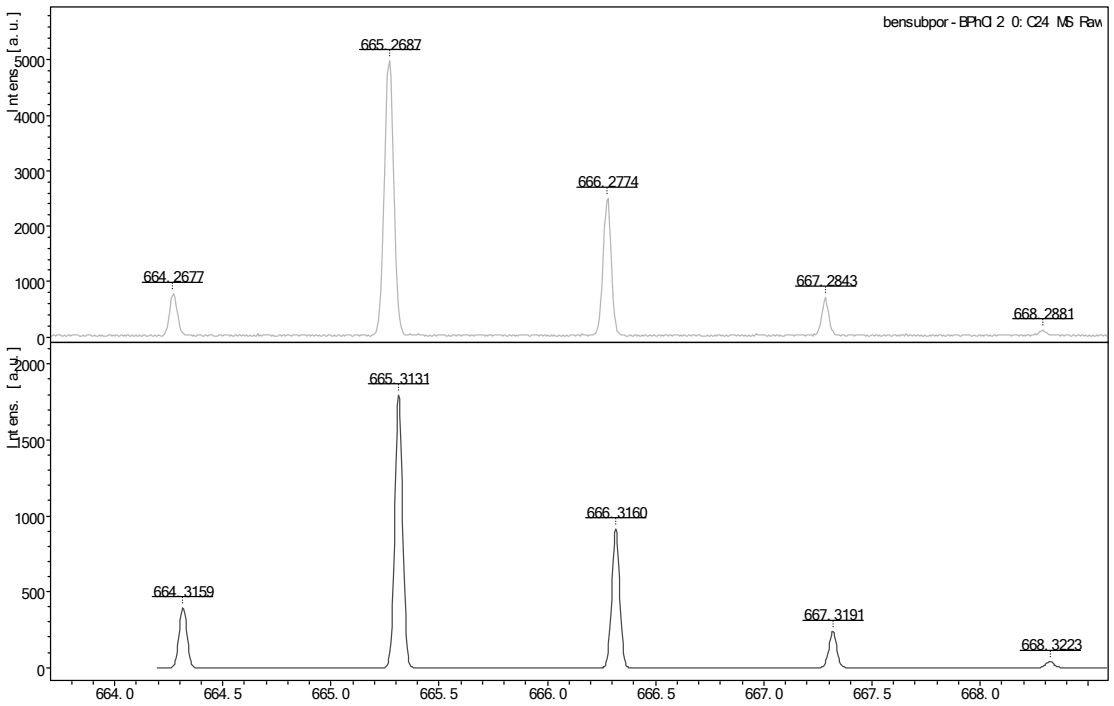

Figure S11. MALDI-TOF-MS of **8**. (Top: observed; Bottom: simulated)

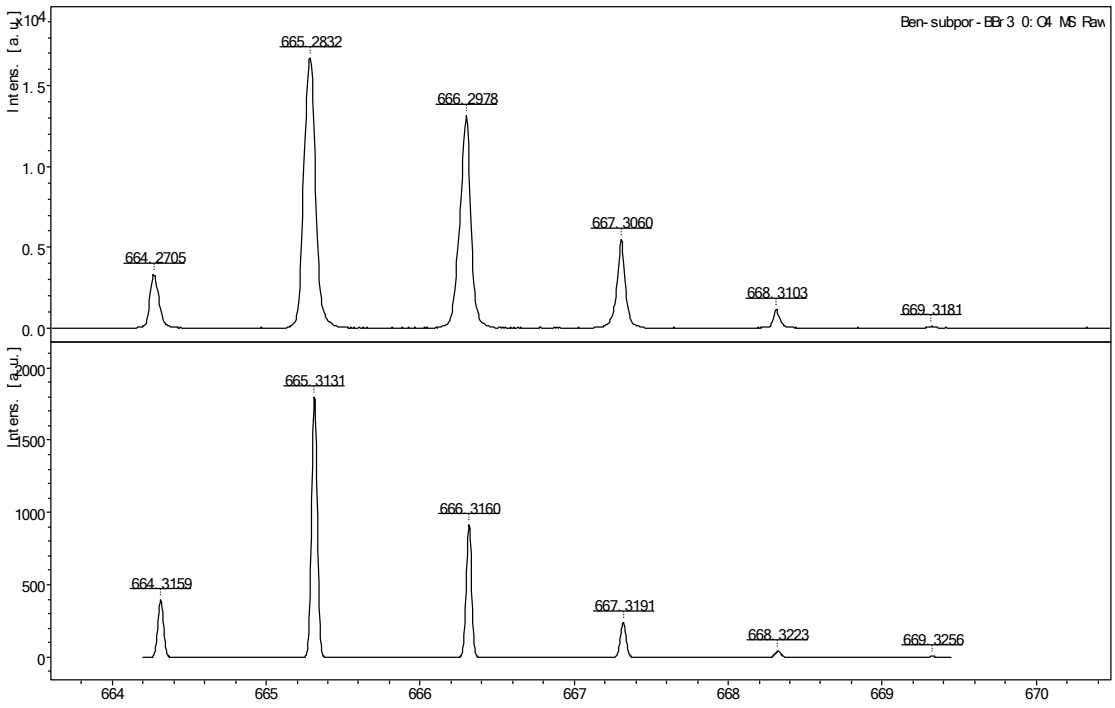

Figure S12. MALDI-TOF-MS of **9**. (Top: observed; Bottom: simulated)

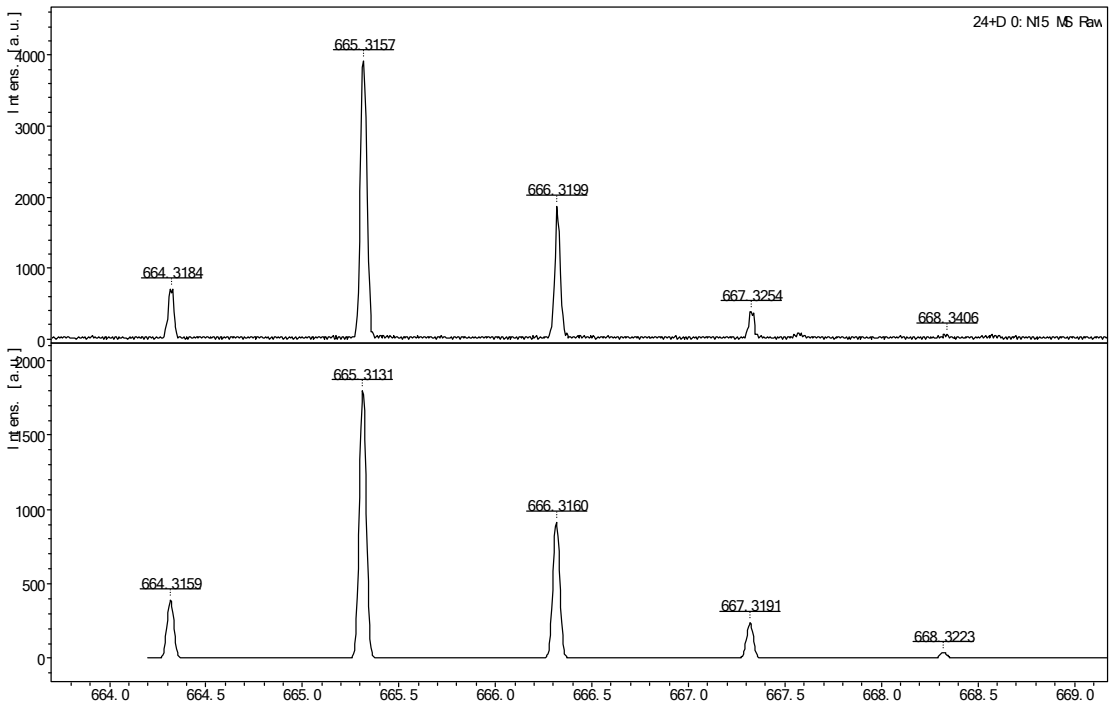

Figure S13. MALDI-TOF-MS of **10**. (Top: observed; Bottom: simulated)

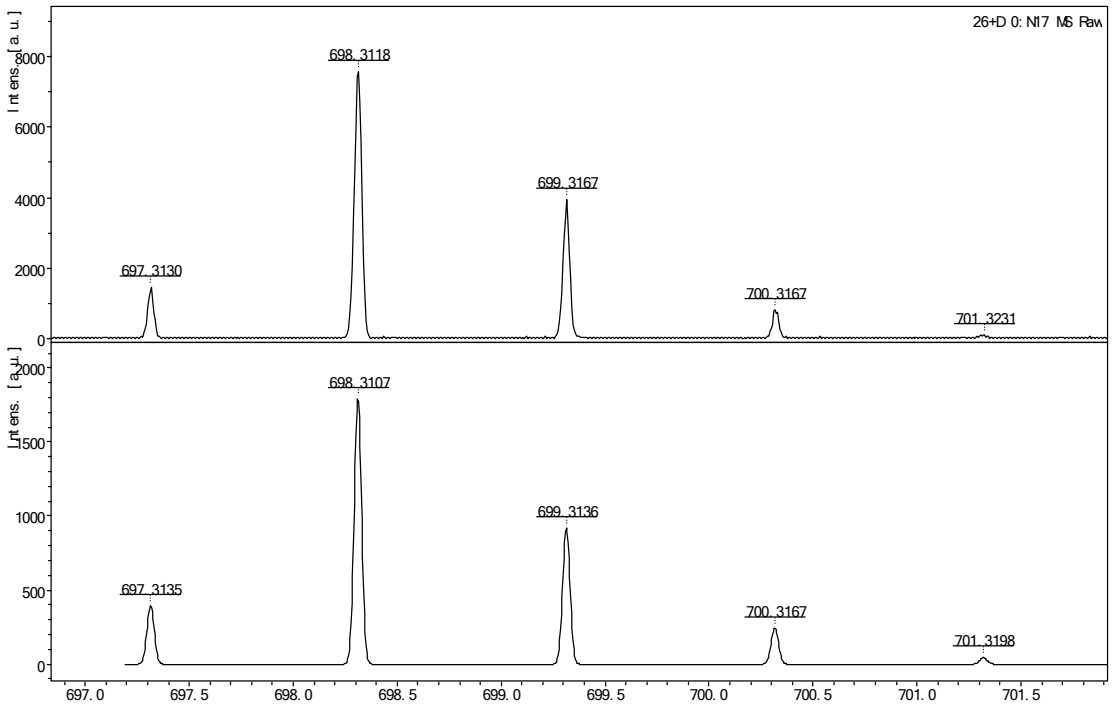

Figure S14. MALDI-TOF-MS of **11**. (Top: observed; Bottom: simulated)

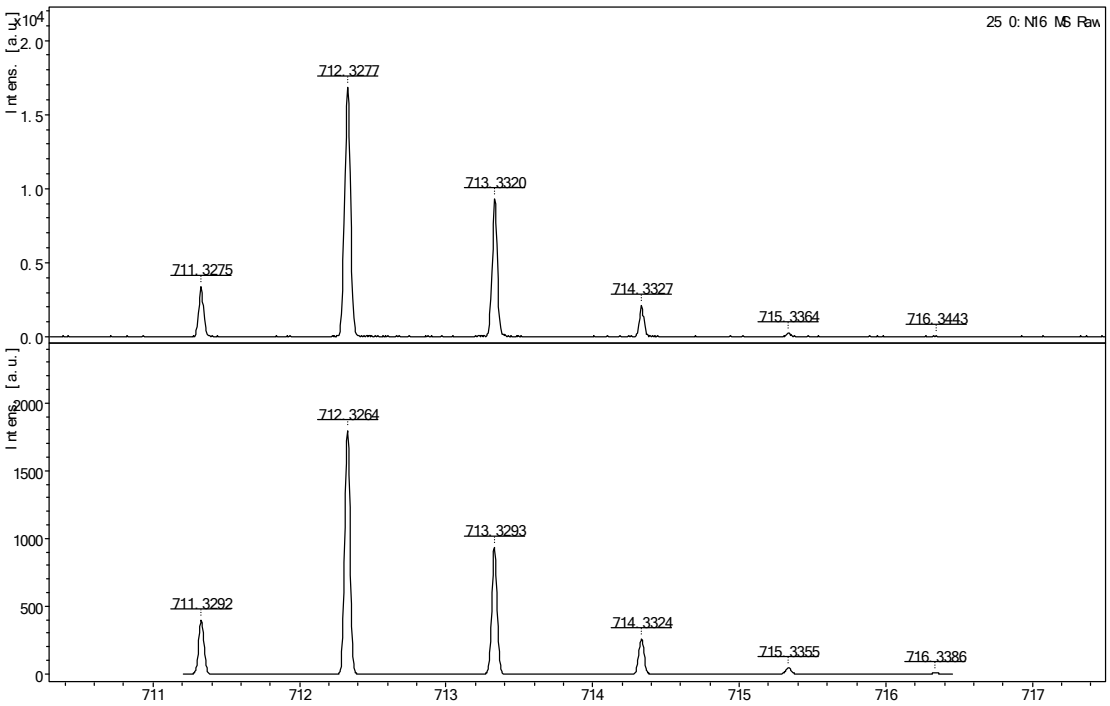

Figure S15. MALDI-TOF-MS of **12**. (Top: observed; Bottom: simulated)

4. Electrochemical Data

Cyclic voltammograms and differential pulse voltammograms were measured in DCM with 0.1 M $^{n}Bu_4NPF_6$. Potentials were determined vs ferrocene/ferrocenium ion by differential pulse voltammograms. Working electrode: glassy carbon. Counter electrode: Pt wire. Reference electrode: $AgNO_3$.

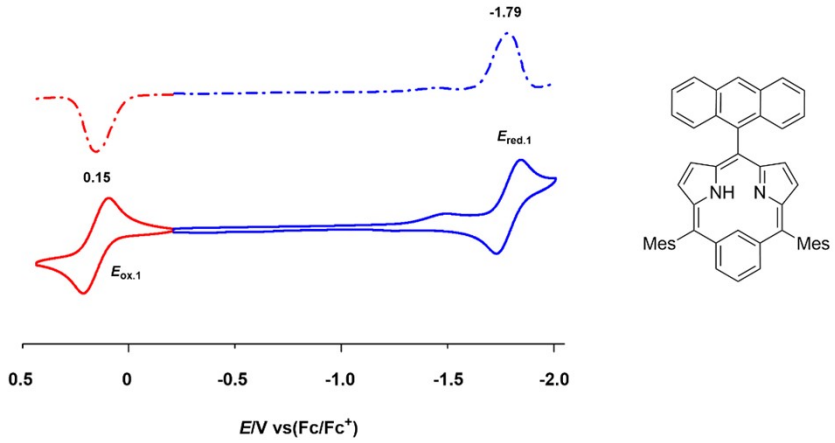

Figure S16. Cyclic voltammogram and differential pulse voltammogram of **6**.

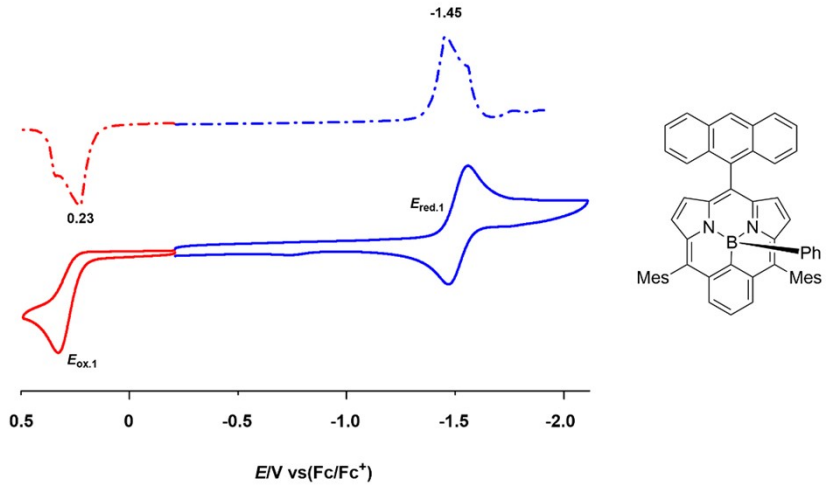

Figure S17. Cyclic voltammogram and differential pulse voltammogram of **8**.

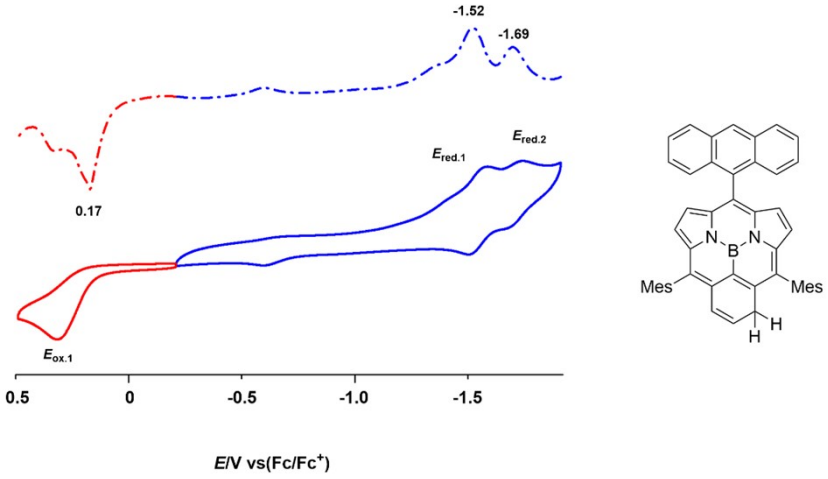

Figure S18. Cyclic voltammogram and differential pulse voltammogram of **9**.

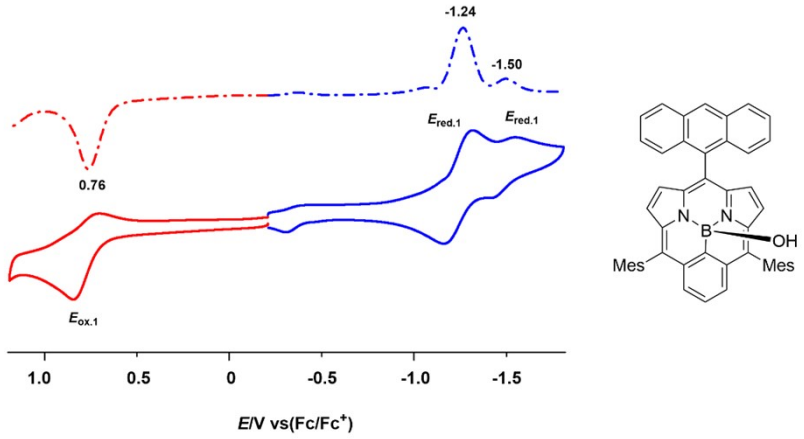

Figure S19. Cyclic voltammogram and differential pulse voltammogram of **10**.

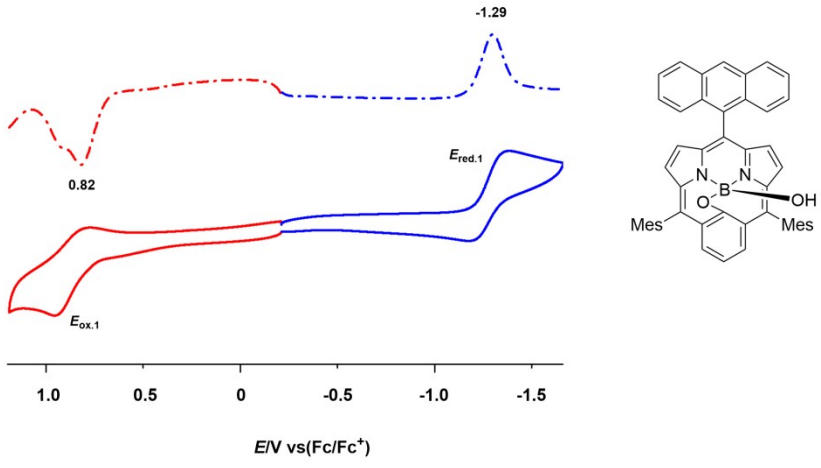

Figure S20. Cyclic voltammogram and differential pulse voltammogram of **11**.

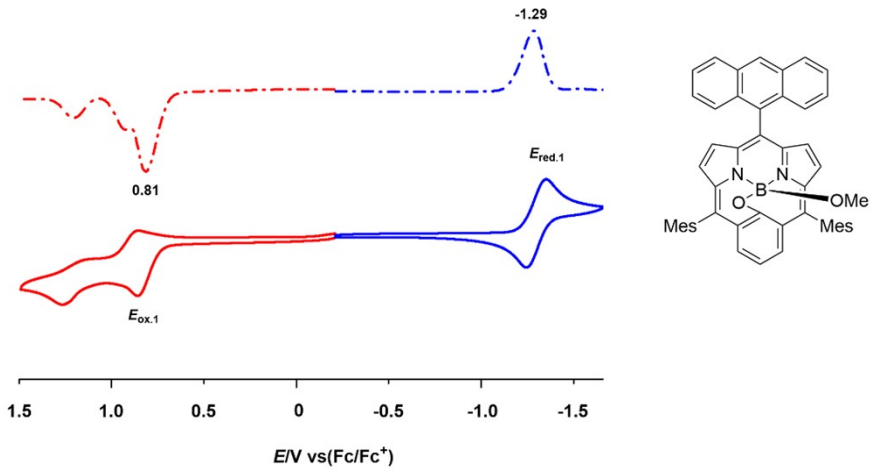

Figure S21. Cyclic voltammogram and differential pulse voltammogram of **12**.

Table S1. Summary of the electrochemical potentials (V) and HOMO–LUMO gaps (eV).

samples	$E_{ox.1}$	$E_{red.1}$	$E_{red.2}$	ΔE_{HL}[b]
6	0.15	-1.79	--	1.94
8	0.23	-1.45	--	1.68
9	0.17	-1.52	-1.69	1.69
10	0.76	-1.24	-1.50	2.00
11	0.82	-1.29	--	2.11
12	0.81	-1.29	--	2.10

[a]Irreversible peaks. [b]ΔE_{HL} = e ($E_{ox.1}$–$E_{red.1}$) [eV]

5. X-Ray Crystal Data

Table S2. Crystal data and structure refinement for **6**.

Identification code	exp_3719	
Empirical formula	C51 H43 N3	
Formula weight	697.88	
Temperature	100.01(10) K	
Wavelength	1.54184 Å	
Crystal system	Monoclinic	
Space group	P 1 21/n 1	
Unit cell dimensions	a = 12.0996(5) Å	α= 90°.
	b = 10.9016(5) Å	β= 96.378(4)°.
	c = 29.2496(12) Å	γ = 90°.
Volume	3834.3(3) $Å^3$	
Z	4	
Density (calculated)	1.209 Mg/m^3	
Absorption coefficient	0.535 mm^{-1}	
F(000)	1480	
Crystal size	0.3 x 0.1 x 0.1 mm^3	
Theta range for data collection	3.040 to 66.597°.	
Index ranges	-14<=h<=8, -12<=k<=12, -29<=l<=34	
Reflections collected	13633	
Independent reflections	6772 [R(int) = 0.0534]	
Completeness to theta = 66.597°	99.9 %	
Absorption correction	Semi-empirical from equivalents	
Max. and min. transmission	1.00000 and 0.70836	
Refinement method	Full-matrix least-squares on F^2	
Data / restraints / parameters	6772 / 0 / 494	
Goodness-of-fit on F^2	1.047	
Final R indices [I>2sigma(I)]	R1 = 0.0575, wR2 = 0.1249	
R indices (all data)	R1 = 0.0889, wR2 = 0.1414	
Extinction coefficient	n/a	
Largest diff. peak and hole	0.266 and -0.458 $e.Å^{-3}$	
CCDC number	2379624	

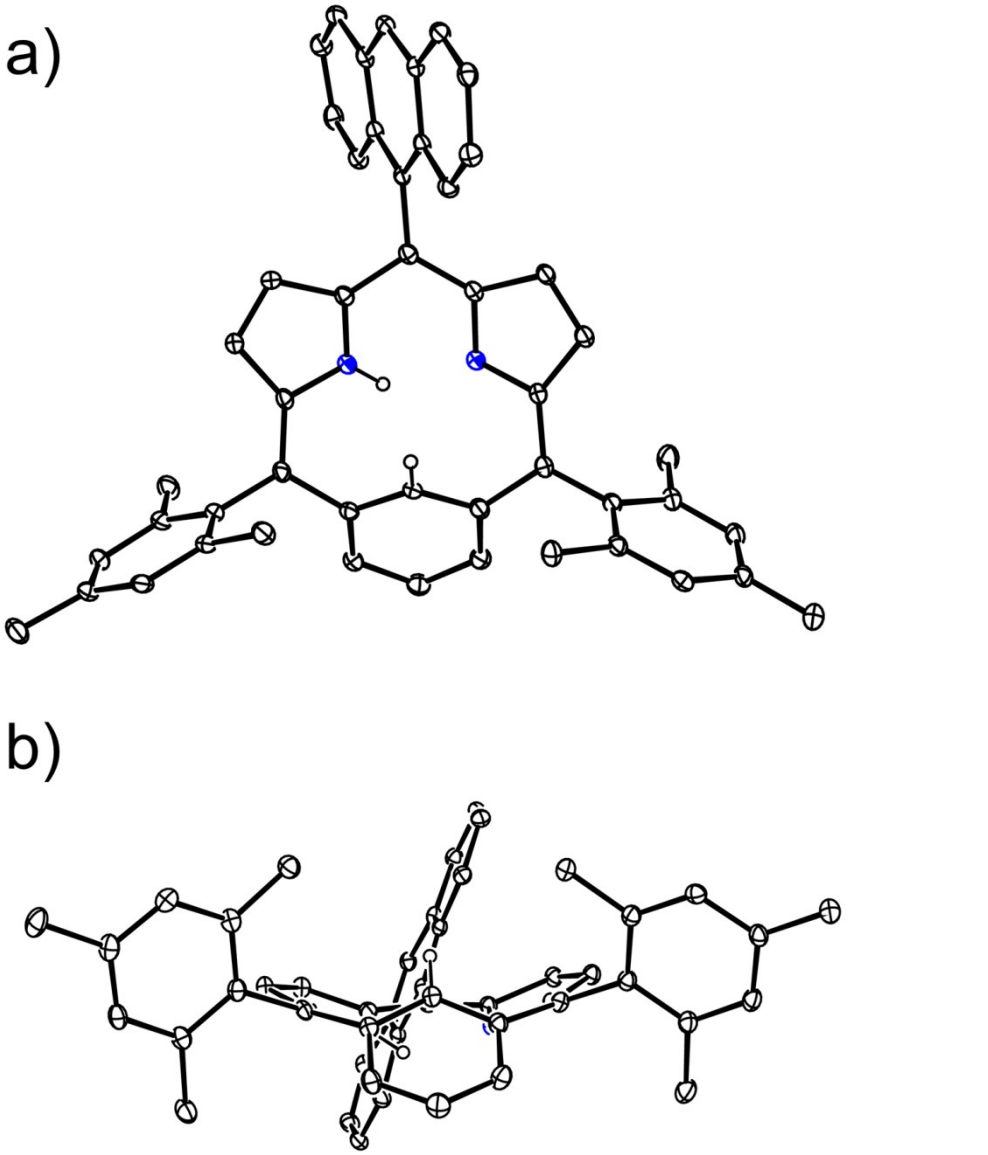

Figure S22. X-ray crystal structure of **6**. (a) Top view and (b) side view. The thermal ellipsoids are 30% probability level.

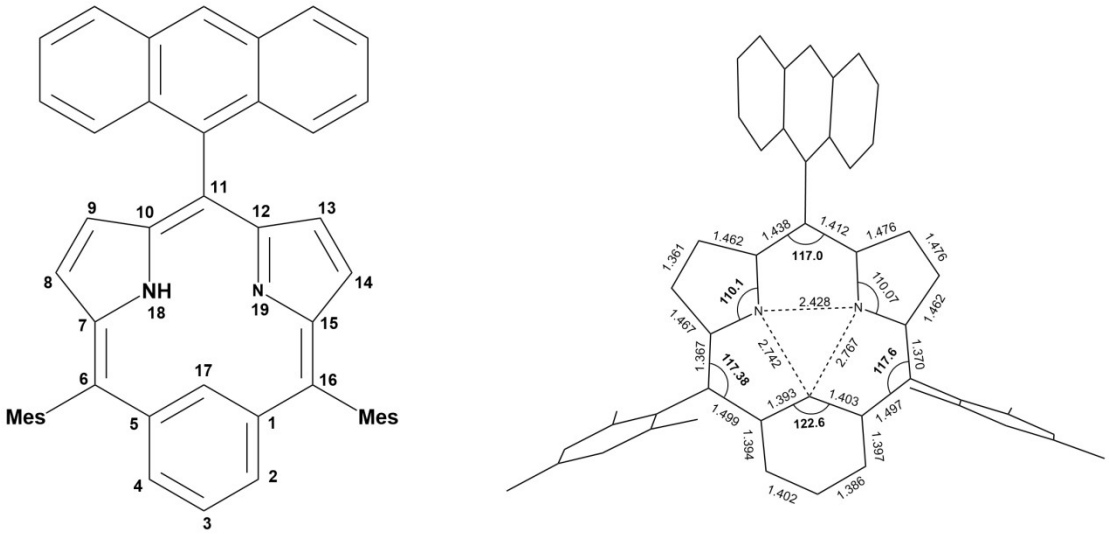

Figure S23. Structural analysis of **6**.

Table S3. Crystal data and structure refinement for **8**.

Identification code	exp_3472_sq	
Empirical formula	C55 H43 B N2	
Formula weight	742.72	
Temperature	100.01(10) K	
Wavelength	1.54184 Å	
Crystal system	Triclinic	
Space group	P-1	
Unit cell dimensions	a = 12.2357(4) Å	α= 78.284(3)°.
	b = 13.4613(5) Å	β= 77.397(3)°.
	c = 14.9649(5) Å	γ = 76.902(3)°.
Volume	2312.08(15) $Å^3$	
Z	2	
Density (calculated)	1.067 Mg/m^3	
Absorption coefficient	0.464 mm^{-1}	
F(000)	784	
Crystal size	0.2 x 0.2 x 0.2 mm^3	
Theta range for data collection	3.066 to 66.600°.	
Index ranges	-14<=h<=14, -16<=k<=14, -17<=l<=13	
Reflections collected	14849	
Independent reflections	8162 [R(int) = 0.0181]	
Completeness to theta = 66.600°	100.0 %	
Absorption correction	Semi-empirical from equivalents	
Max. and min. transmission	1.00000 and 0.89352	
Refinement method	Full-matrix least-squares on F^2	
Data / restraints / parameters	8162 / 0 / 529	
Goodness-of-fit on F^2	1.036	
Final R indices [I>2sigma(I)]	R1 = 0.0406, wR2 = 0.0999	
R indices (all data)	R1 = 0.0460, wR2 = 0.1039	
Extinction coefficient	n/a	
Largest diff. peak and hole	0.689 and -0.254 $e.Å^{-3}$	
CCDC number	2379625	

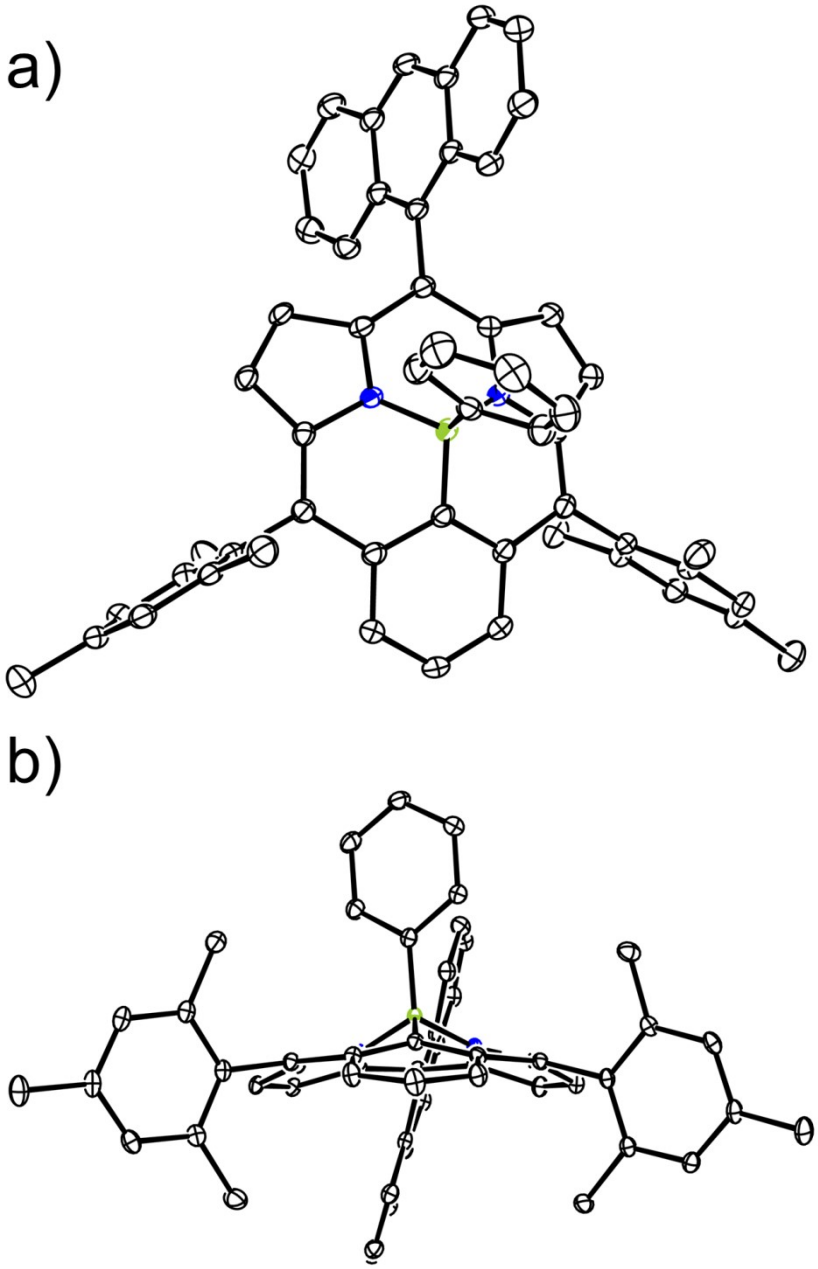

Figure S24. X-ray crystal structure of **8**. (a) Top view and (b) side view. The thermal ellipsoids are 30% probability level.

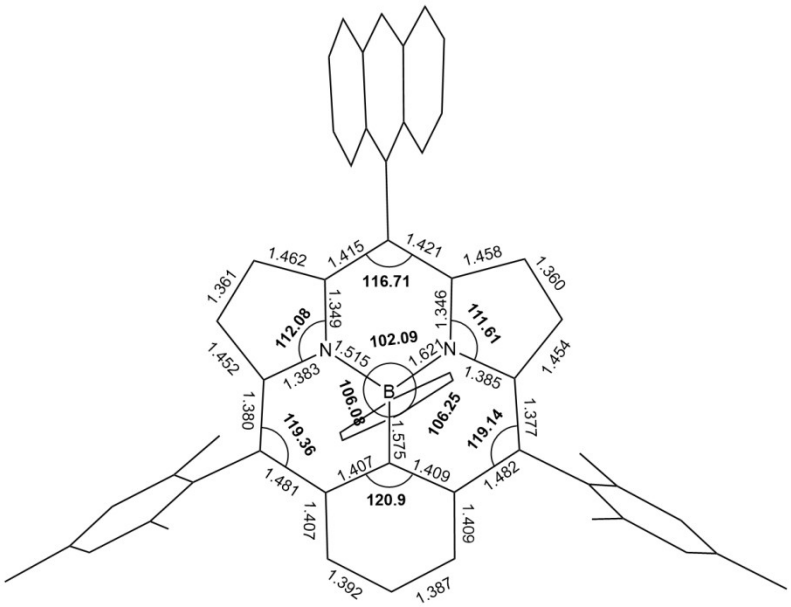

Figure S25. Structural analysis of **8**.

Table S4. Crystal data and structure refinement for **9**.

Identification code	exp_3473_sq	
Empirical formula	C49 H39 B N2	
Formula weight	666.63	
Temperature	100.01(10) K	
Wavelength	1.54184 Å	
Crystal system	Triclinic	
Space group	P-1	
Unit cell dimensions	a = 11.6677(12) Å	α= 103.399(7)°.
	b = 12.7694(11) Å	β= 109.908(8)°.
	c = 14.5328(8) Å	γ = 94.935(7)°.
Volume	1948.0(3) $Å^3$	
Z	2	
Density (calculated)	1.137 Mg/m^3	
Absorption coefficient	0.495 mm^{-1}	
F(000)	704	
Crystal size	0.05 x 0.05 x 0.05 mm^3	
Theta range for data collection	3.368 to 66.600°.	
Index ranges	-13<=h<=9, -14<=k<=15, -17<=l<=17	
Reflections collected	11838	
Independent reflections	6887 [R(int) = 0.0516]	
Completeness to theta = 66.600°	99.9 %	
Absorption correction	Semi-empirical from equivalents	
Max. and min. transmission	1.00000 and 0.76183	
Refinement method	Full-matrix least-squares on F^2	
Data / restraints / parameters	6887 / 0 / 475	
Goodness-of-fit on F^2	1.047	
Final R indices [I>2sigma(I)]	R1 = 0.0815, wR2 = 0.2160	
R indices (all data)	R1 = 0.1166, wR2 = 0.2447	
Extinction coefficient	n/a	
Largest diff. peak and hole	0.541 and -0.265 $e.Å^{-3}$	
CCDC number	2379626	

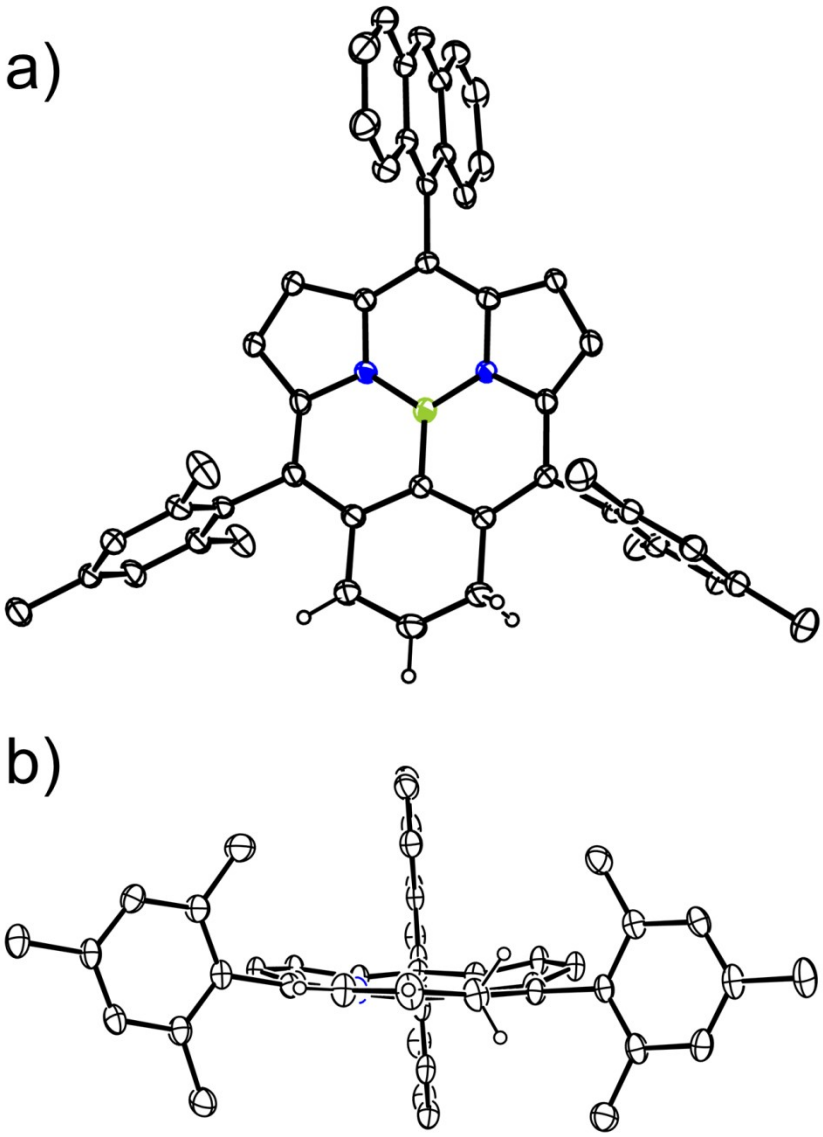

Figure S26. X-ray crystal structure of **9**. (a) Top view and (b) side view. The thermal ellipsoids are 30% probability level.

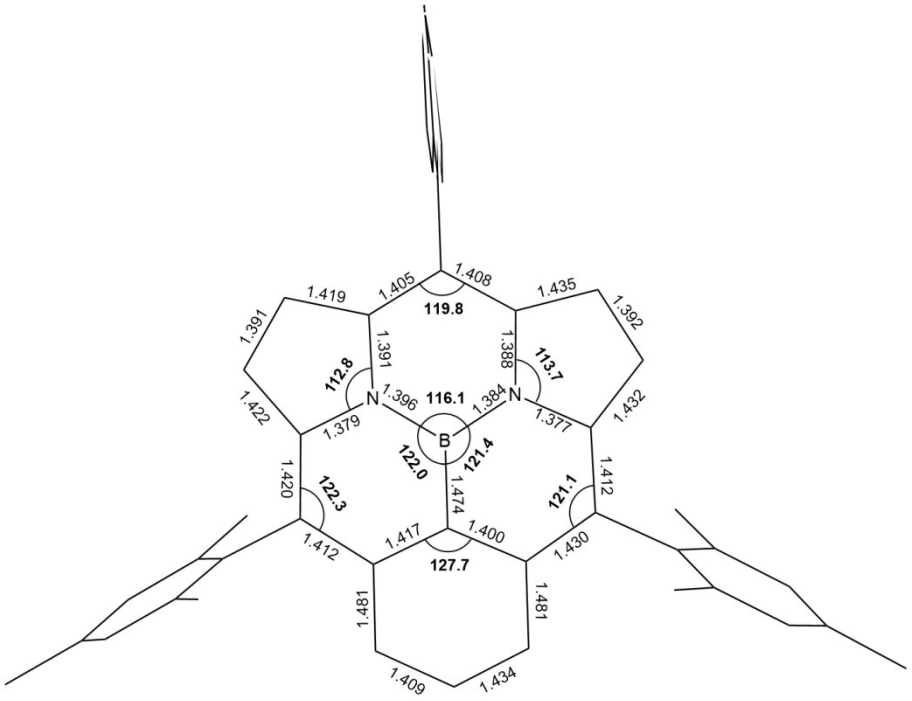

Figure S27. Structural analysis of **9**

Table S5. Crystal data and structure refinement for **10**.

Identification code	exp_3736_sq	
Empirical formula	C49 H39 B N2 O	
Formula weight	682.63	
Temperature	99.98(10) K	
Wavelength	1.54184 Å	
Crystal system	Triclinic	
Space group	P-1	
Unit cell dimensions	a = 11.9190(12) Å	α= 104.186(8)°.
	b = 12.5825(11) Å	β= 110.328(9)°.
	c = 14.8081(16) Å	γ = 96.071(8)°.
Volume	1974.0(4) $Å^3$	
Z	2	
Density (calculated)	1.148 Mg/m^3	
Absorption coefficient	0.519 mm^{-1}	
F(000)	720	
Crystal size	0.1 x 0.05 x 0.05 mm^3	
Theta range for data collection	3.339 to 66.599°.	
Index ranges	-14<=h<=12, -14<=k<=14, -17<=l<=17	
Reflections collected	12275	
Independent reflections	6960 [R(int) = 0.0816]	
Completeness to theta = 66.599°	99.8 %	
Absorption correction	Semi-empirical from equivalents	
Max. and min. transmission	1.00000 and 0.59263	
Refinement method	Full-matrix least-squares on F^2	
Data / restraints / parameters	6960 / 6 / 485	
Goodness-of-fit on F^2	1.027	
Final R indices [I>2sigma(I)]	R1 = 0.0818, wR2 = 0.1879	
R indices (all data)	R1 = 0.1507, wR2 = 0.2274	
Extinction coefficient	n/a	
Largest diff. peak and hole	0.334 and -0.663 $e.Å^{-3}$	
CCDC number	2379627	

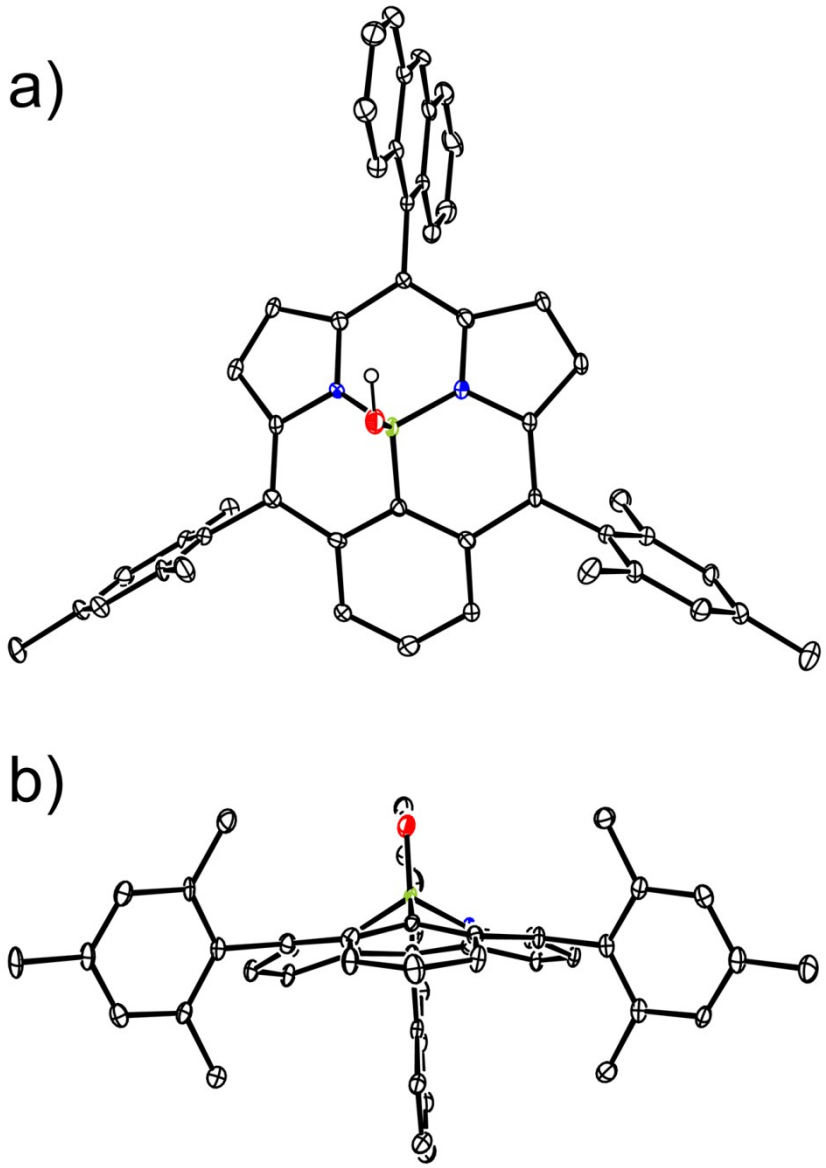

Figure S28. X-ray crystal structure of **10**. (a) Top view and (b) side view. The thermal ellipsoids are 30% probability level.

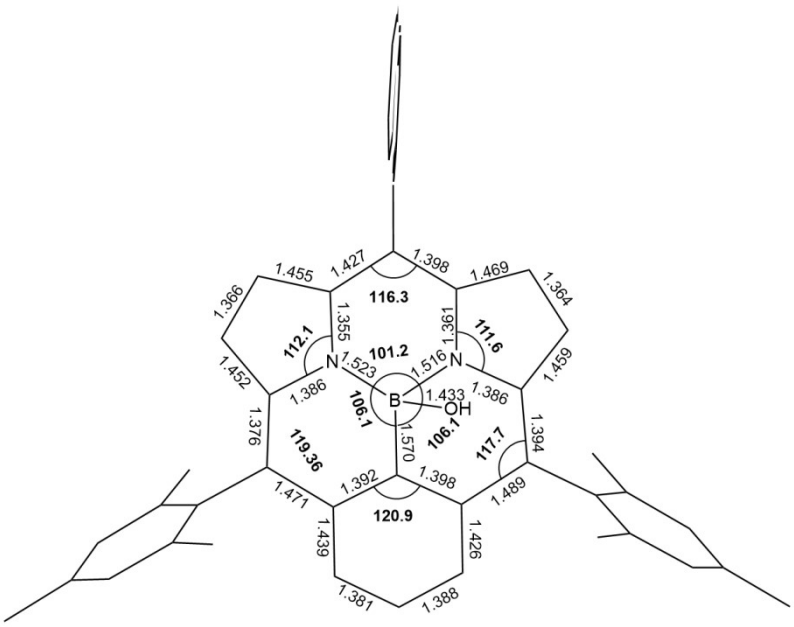

Figure S29. Structural analysis of **10.**

Table S6. Crystal data and structure refinement for **11**.

Identification code	exp_3517_sq	
Empirical formula	C49 H39 B N2 O2	
Formula weight	698.63	
Temperature	100.00(10) K	
Wavelength	1.54184 Å	
Crystal system	Monoclinic	
Space group	P 1 21/c 1	
Unit cell dimensions	a = 13.211(2) Å	α= 90°.
	b = 20.856(2) Å	β= 114.86(2)°.
	c = 15.732(3) Å	γ = 90°.
Volume	3932.9(11) $Å^3$	
Z	4	
Density (calculated)	1.180 Mg/m^3	
Absorption coefficient	0.552 mm^{-1}	
F(000)	1472	
Crystal size	0.1 x 0.05 x 0.05 mm^3	
Theta range for data collection	3.688 to 66.597°.	
Index ranges	-15<=h<=15, -24<=k<=24, -18<=l<=18	
Reflections collected	27391	
Independent reflections	6939 [R(int) = 0.1325]	
Completeness to theta = 66.597°	100.0 %	
Absorption correction	Semi-empirical from equivalents	
Max. and min. transmission	1.00000 and 0.33807	
Refinement method	Full-matrix least-squares on F^2	
Data / restraints / parameters	6939 / 0 / 498	
Goodness-of-fit on F^2	0.778	
Final R indices [I>2sigma(I)]	R1 = 0.0543, wR2 = 0.1082	
R indices (all data)	R1 = 0.1272, wR2 = 0.1332	
Extinction coefficient	n/a	
Largest diff. peak and hole	0.253 and -0.313 $e.Å^{-3}$	
CCDC number	2379628	

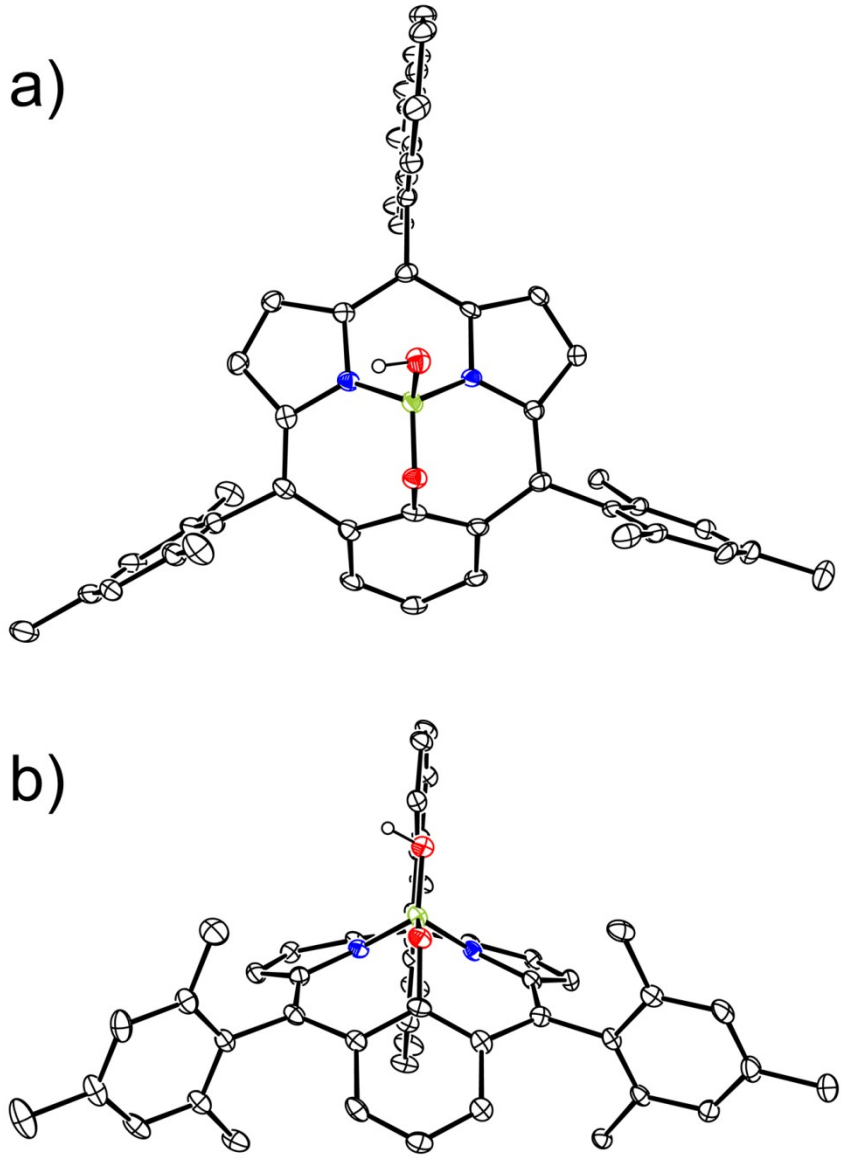

Figure S30. X-ray crystal structure of **11**. (a) Top view and (b) side view. The thermal ellipsoids are 30% probability level.

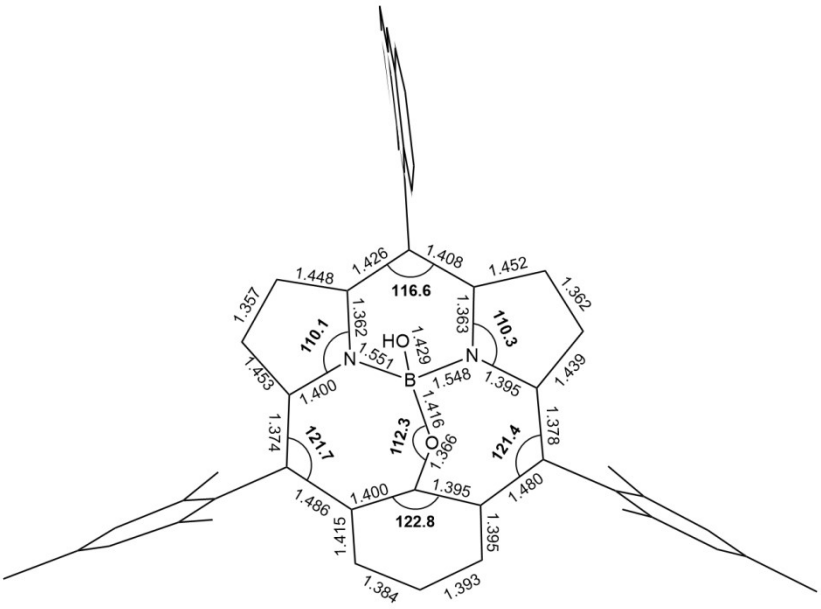

Figure S31. Structural analysis of **11**.

Table S7. Crystal data and structure refinement for **12**.

Identification code	exp_3498_sq	
Empirical formula	C50 H41 B N2 O2	
Formula weight	712.66	
Temperature	100.00(10) K	
Wavelength	1.54184 Å	
Crystal system	Triclinic	
Space group	P-1	
Unit cell dimensions	a = 14.4553(6) Å	α= 92.220(3)°.
	b = 15.1300(6) Å	β= 94.235(3)°.
	c = 21.0270(7) Å	γ = 98.658(4)°.
Volume	4528.2(3) $Å^3$	
Z	4	
Density (calculated)	1.045 Mg/m^3	
Absorption coefficient	0.487 mm^{-1}	
F(000)	1504	
Crystal size	0.2 x 0.2 x 0.05 mm^3	
Theta range for data collection	2.958 to 66.600°.	
Index ranges	-17<=h<=17, -17<=k<=18, -17<=l<=25	
Reflections collected	29740	
Independent reflections	15982 [R(int) = 0.0562]	
Completeness to theta = 66.600°	99.9 %	
Absorption correction	Semi-empirical from equivalents	
Max. and min. transmission	1.00000 and 0.62092	
Refinement method	Full-matrix least-squares on F^2	
Data / restraints / parameters	15982 / 78 / 1005	
Goodness-of-fit on F^2	1.029	
Final R indices [I>2sigma(I)]	R1 = 0.0622, wR2 = 0.1525	
R indices (all data)	R1 = 0.0881, wR2 = 0.1684	
Extinction coefficient	n/a	
Largest diff. peak and hole	0.401 and -0.704 $e.Å^{-3}$	
CCDC number	2379629	

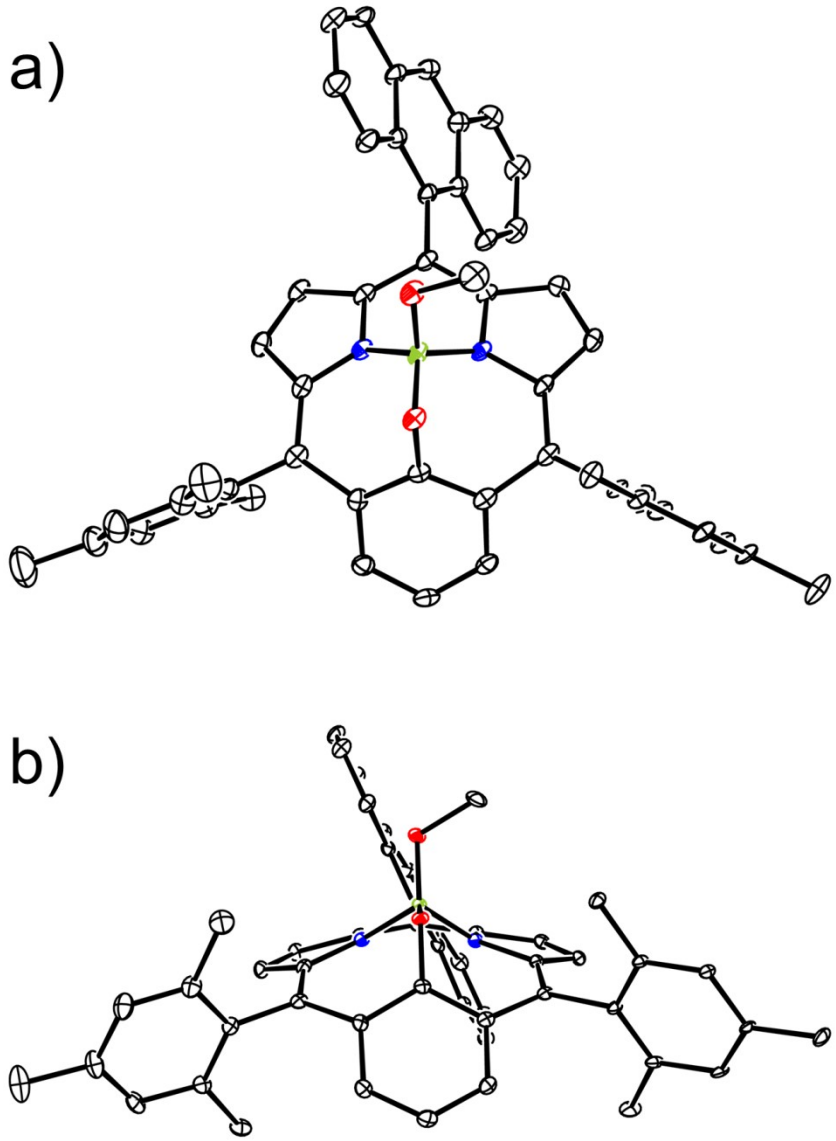

Figure S32. X-ray crystal structure of **12**. (a) Top view and (b) side view. The thermal ellipsoids are 30% probability level.

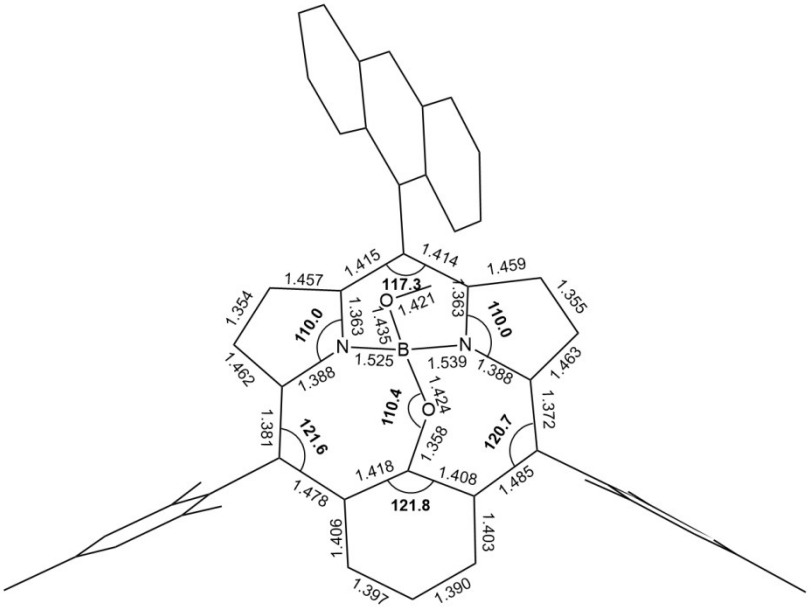

Figure S33. Structural analysis of **12.**

6. DFT Calculation

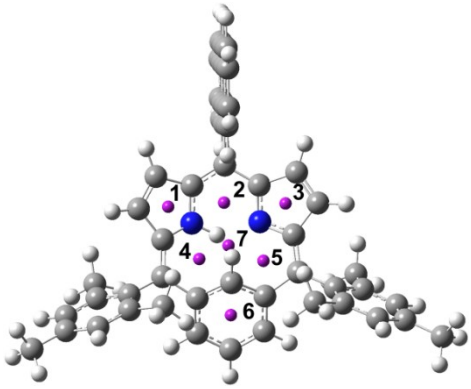

position	1	2	3	4	5	6	7
6	-4.0287	2.0801	-2.6389	0.0419	-0.6589	-8.0409	1.5118

Figure S34. NICS values at various positions of **6** on the optimized structure.

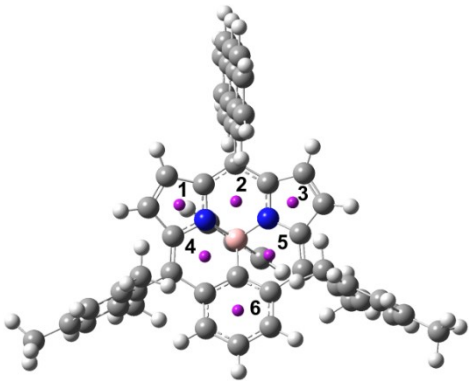

position	1	2	3	4	5	6
8	-1.8352	1.0489	-2.2078	4.8300	5.5793	-2.3629

Figure S35. NICS values at various positions of **8** on the optimized structure.

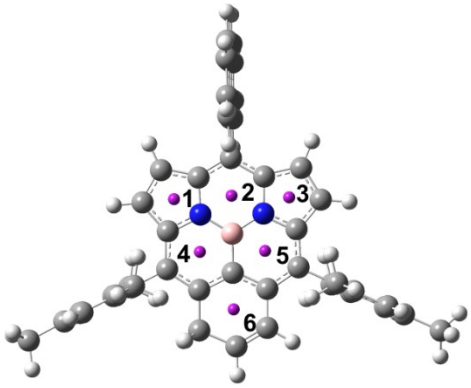

position	1	2	3	4	5	6
9	-13.5152	-9.5777	-14.5315	-11.6418	-10.4852	9.0935

Figure S36. NICS values at various positions of **9** on the optimized structure.

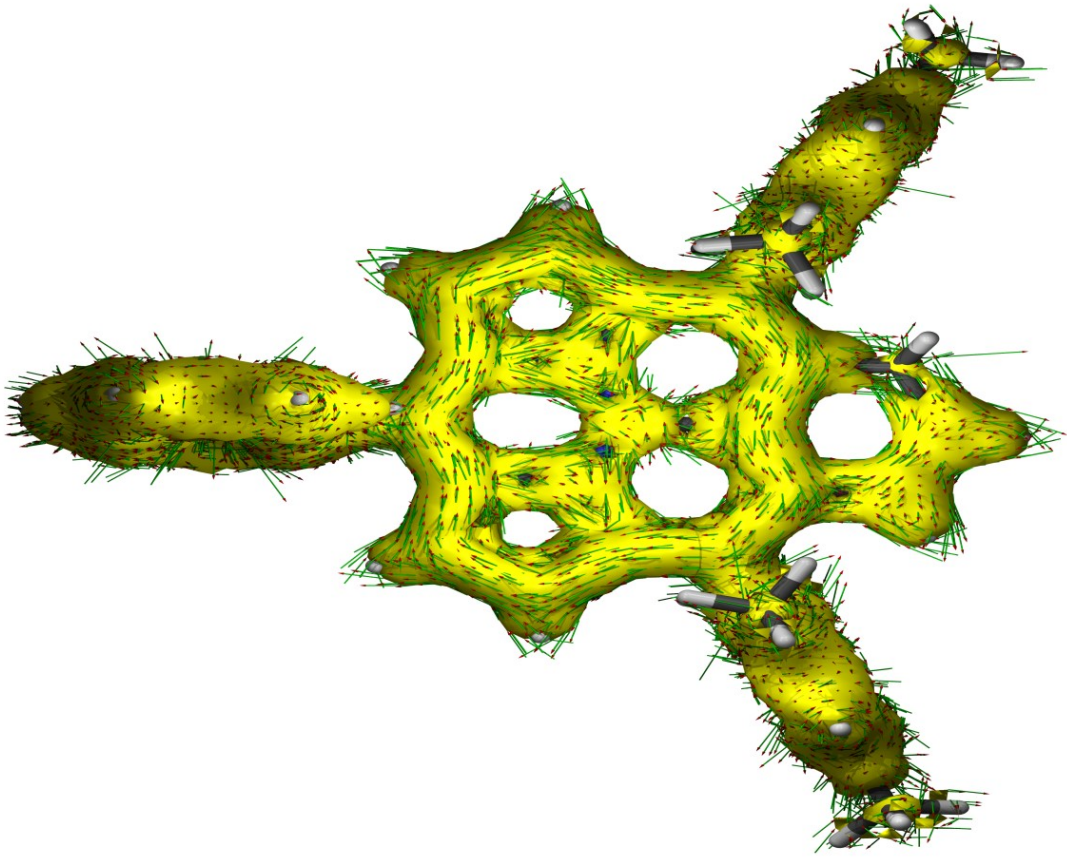

Figure S37. ACID plot of **9** at isosurface value of 0.04. The external magnetic field was applied in the direction from the back of the paper to the surface.

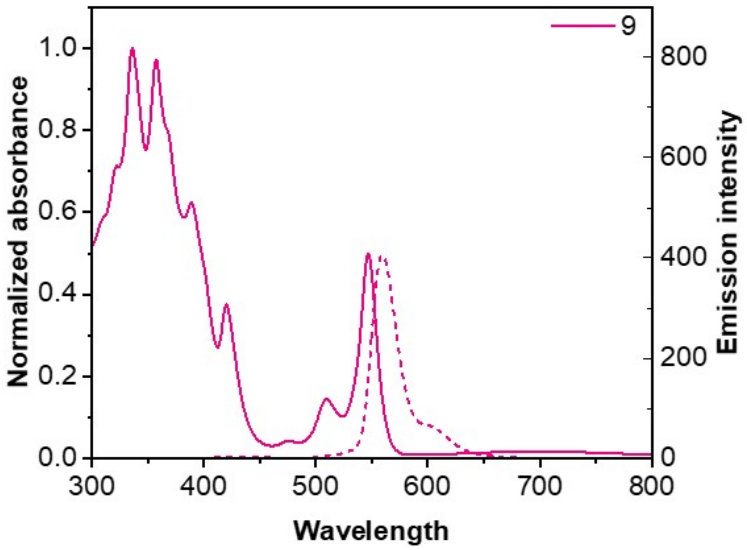

Figure S38. UV-Vis and fluorescence spectra of **9** with solid and dotted lines, respectively.

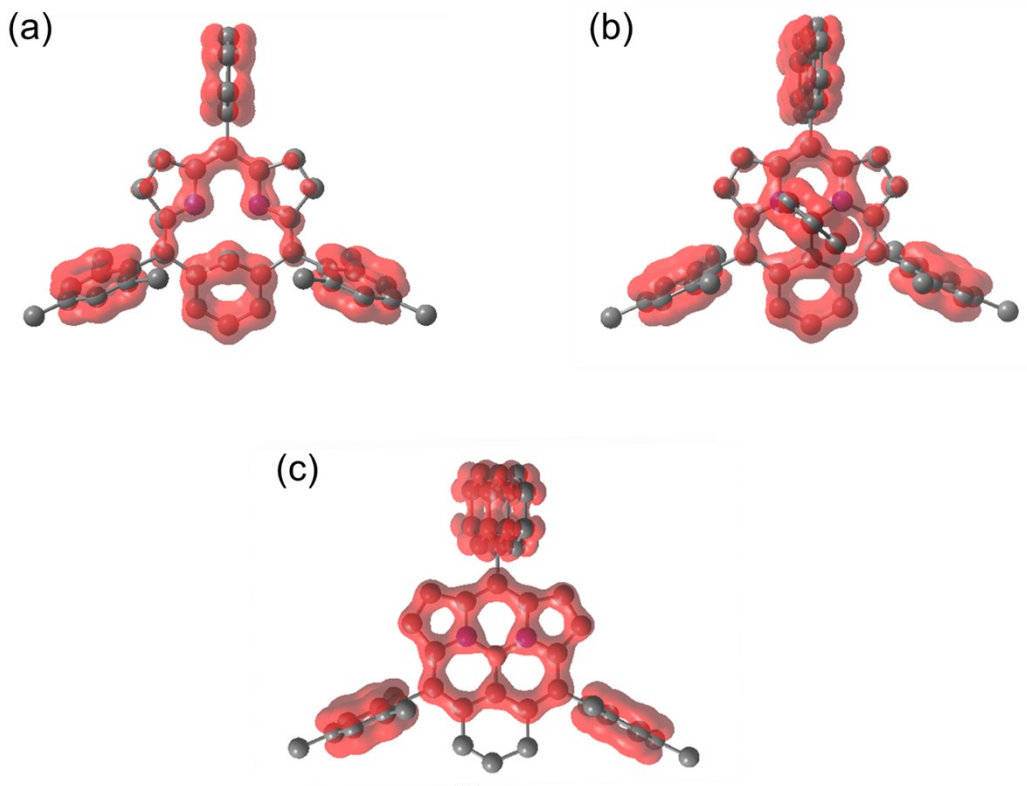

Figure S39. EDDB plots of (a) **6**, (b) **8**, and (c) **9**, where cyclic π-conjugation pathways are visualized with red-colored surface with an isovalue of 0.02.

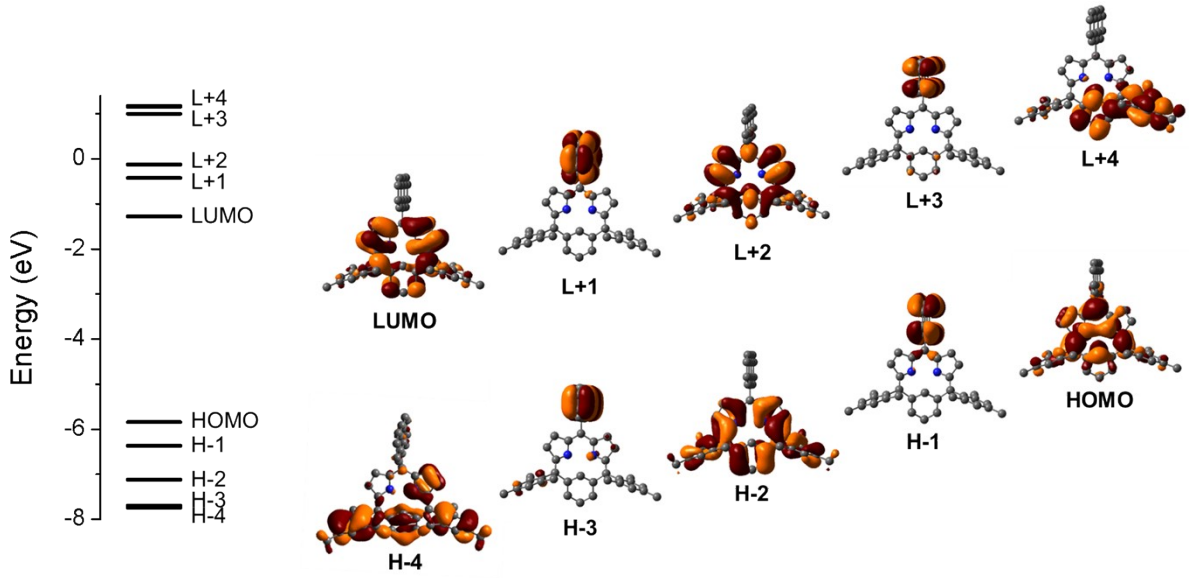

Figure S40. MO energy diagram and electron density distribution of **6**.

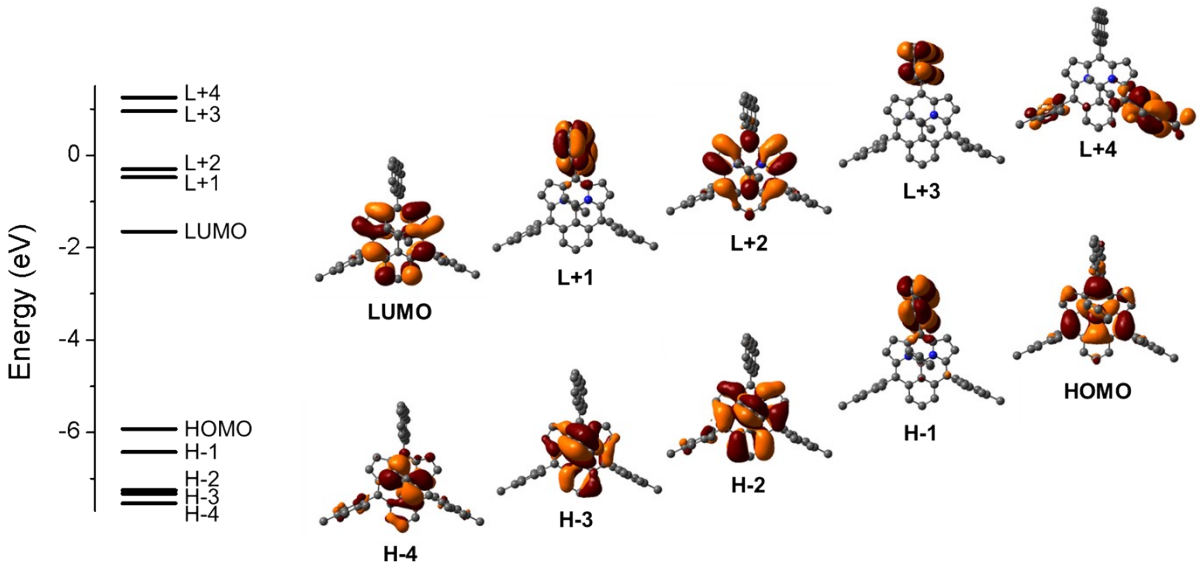

Figure S41. MO energy diagram and electron density distribution of **8**.

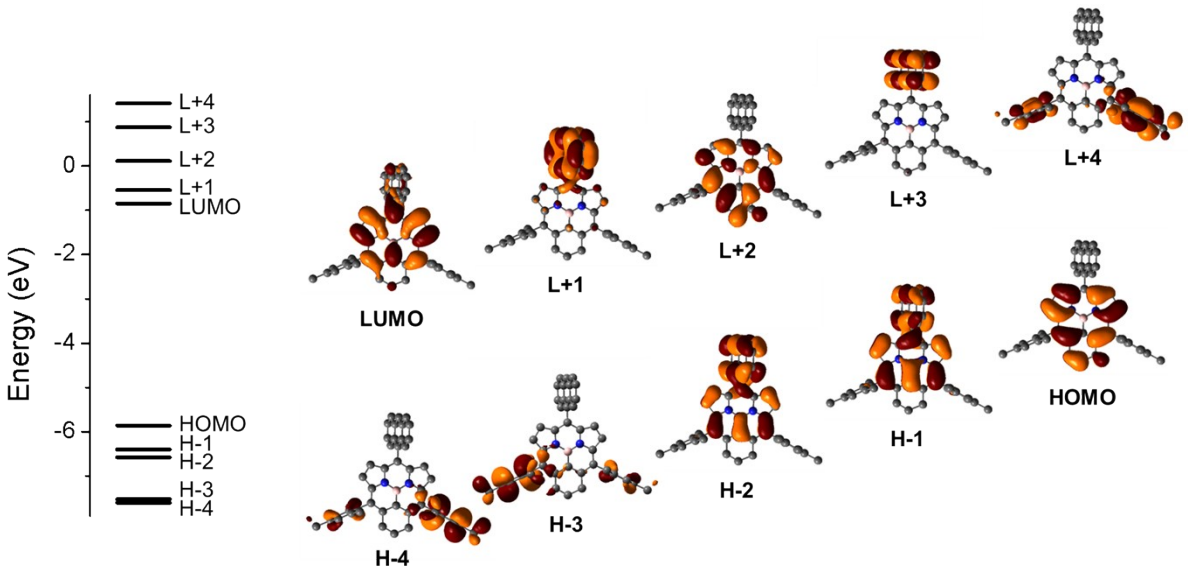

Figure S42. MO energy diagram and electron density distribution of **9**.

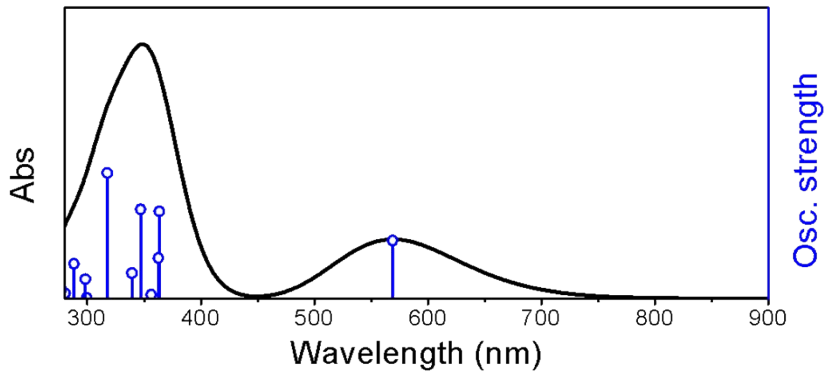

No.	Wavelength (nm)	Osc. Strength	Major contributions
1	568.9	0.1501	HOMO→LUMO (95%)
2	363.3	0.2253	HOMO→L+1 (17%), HOMO→L+2 (58%), H-1→LUMO (8%), H-1→L+1 (9%)
3	362.5	0.1045	H-1→LUMO (76%), HOMO→L+1 (8%)
4	356.2	0.0099	HOMO→L+1 (65%), HOMO→L+2 (23%)
5	346.3	0.2303	H-2→LUMO (48%), H-1→L+1 (11%) , H-8→LUMO (9%), H-7→LUMO (7%)
6	339.2	0.0658	H-1→L+1 (68%), H-8→LUMO (9%)
7	317.4	0.3238	H-8→LUMO (10%), H-4→LUMO (14%), H-2→LUMO (38%), H-7→LUMO (9%)

Figure S43. Simulated absorption spectrum and MO contributions on electronic transitions of **6** (Contributions less than 6% are omitted for clarity).

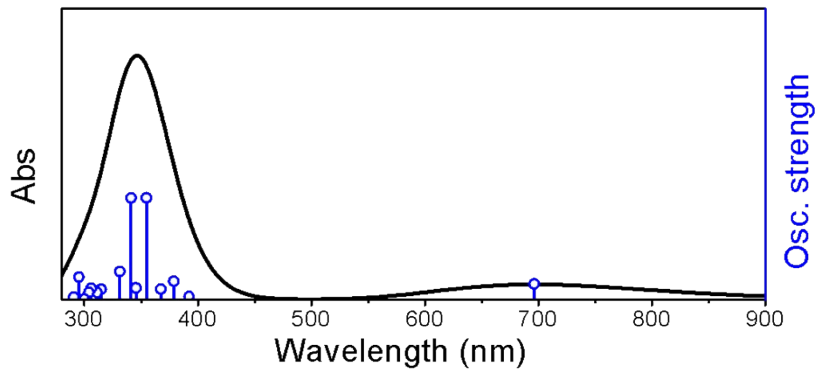

No.	Wavelength (nm)	Osc. Strength	Major contributions
1	696.2	0.0544	HOMO→LUMO (96%)
2	392.2	0.0107	H-1→LUMO (92%)
3	378.8	0.0635	H-2→LUMO (18%), HOMO→L+2 (66%)
4	367.2	0.0364	H-9→LUMO (22%), H-6→LUMO (18%), H-5→LUMO (17%), H-4→LUMO (22%)
5	354.7	0.3499	H-2→LUMO (17%), H-1→L+1 (25%), HOMO→L+1 (53%)
6	345.4	0.0401	H-3→LUMO (52%), H-2→LUMO (32%)
7	341.1	0.3495	H-3→LUMO (24%), H-1→L+1 (26%), HOMO→L+1 (29%)

Figure S44. Simulated absorption spectrum and MO contributions on electronic transitions of **8** (Contributions less than 6% are omitted for clarity).

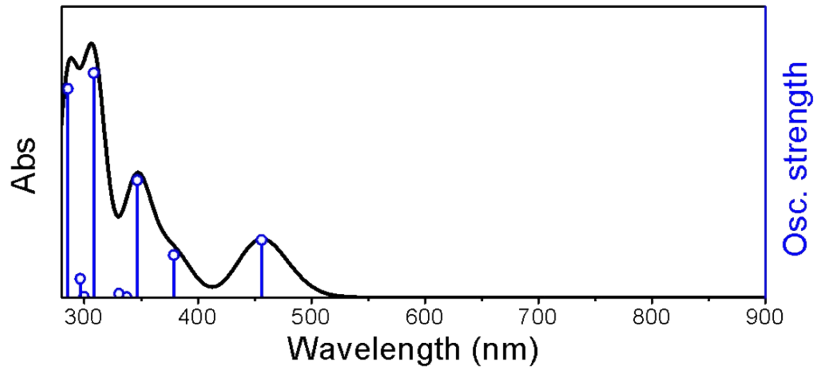

No.	Wavelength (nm)	Osc. Strength	Major contributions
1	456.1	0.1508	HOMO→LUMO (84%), H-1→L+2 (7%)
2	378.7	0.111	H-2→LUMO (10%), H-1→LUMO (61%), HOMO→L+2 (25%)
3	346.7	0.3067	H-2→LUMO (21%), H-2→L+1 (27%), H-1→L+1 (32%), HOMO→L+2 (10%)
4	337.4	0.0013	HOMO→L+1 (91%)
5	330.3	0.0104	H-2→LUMO (48%), H-2→L+1 (18%), H-1→LUMO (15%), H-1→L+1 (16%)
6	308.2	0.587	H-2→LUMO (18%), H-1→LUMO (13%), HOMO→L+2 (55%)
7	299.7	0.0024	H-7→L+1 (44%), H-2→L+3 (25%), H-1→L+3 (18%)

Figure S45. Simulated absorption spectrum and MO contributions on electronic transitions of **9** (Contributions less than 6% are omitted for clarity).

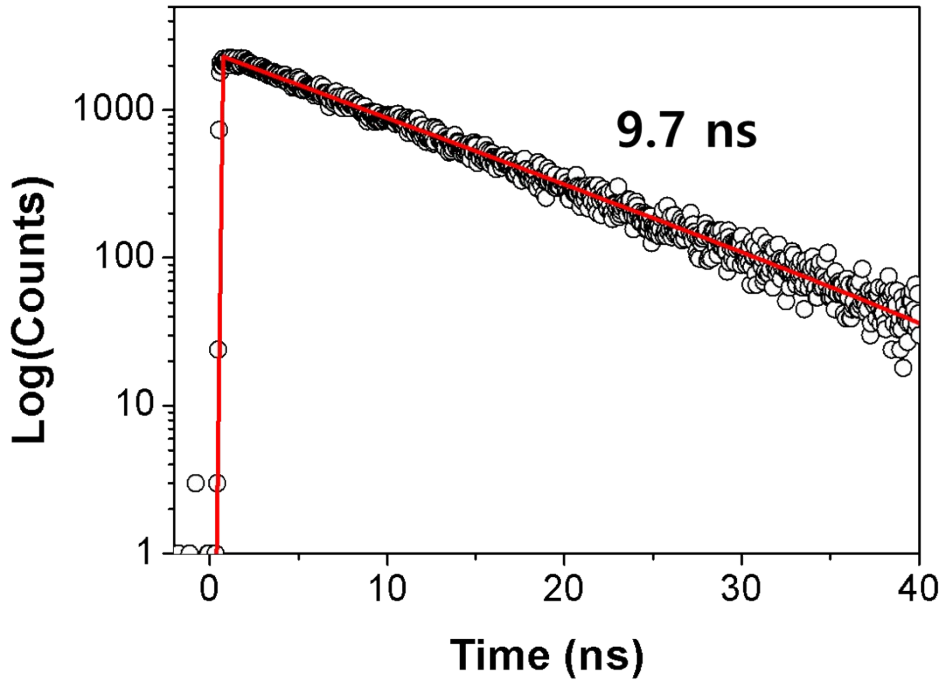

Figure S46. Fluorescence decay profile of **9** in toluene at 560 nm (Photoexcitation at 420 nm).

Transient absorption measurement The femtosecond transient absorption (fs-TA) spectrometer consisted of an optical detection system and an optical parametric amplifier (OPA; Palitra, Quantronix) pumped by a Ti:sapphire regenerative amplifier system (Integra-C, Quantronix) operating at a 1 kHz repetition rate. White light continuum (WLC) probe pulses were generated using a sapphire window (4 mm thick). The intensities of the spectrally dispersed WLC probe pulses were monitored using a high-speed spectrometer (Ultrafast Systems). The cross-correlation full-width at half maximum in the pump-probe experiments was <200 fs. The nanosecond transient absorption (ns-TA) data were measured with the commercial spectrometer (EOS; Ultrafast Systems). After the TA experiments, the absorption spectra of all compounds were carefully examined to determine the presence of artifacts caused by any degradation or photo-oxidation of the samples (Z-202308028841 at the Research Support Center for Bio-Bigdata Analysis and Utilization of Biological Resources).

Computational methods Quantum mechanical calculations were performed by the Gaussian 16, Revision A.03 program suite. All (TD)DFT calculations were performed with camB3LYP/6-31(d,p) with dispersion correction method, DFT-D3(BJ).